Thermal stability characterization of tunneling magneto resistive structure for data storage applications

Mr. Pornchai Rakpongsiri

A Dissertation Submitted in Partial Fulfillment of the Requirements
for the Degree of Doctor of Philosophy in Nanoscience and Technology
Inter-Department of Nanoscience and Technology
Graduate School
Chulalongkorn University
Academic Year 2018

การวิเคราะห์ความเสถียรเชิงความร้อนของโครงสร้างแบบทันเนอริงแมกนิโตรีซิสทิฟเพื่อประยุกต์ใช้งานด้านการเก็บข้อมูล

นายพรชัย รักษ์พงษ์สิริ

วิทยานิพนธ์นี้เป็นส่วนหนึ่งของการศึกษาตามหลักสูตรปริญญาวิทยาศาสตรดุษฎีบัณฑิต
สาขาวิชาวิทยาศาสตร์นาโนและเทคโนโลยี สหสาขาวิชาวิทยาศาสตร์นาโนและเทคโนโลยี
บัณฑิตวิทยาลัย จุฬาลงกรณ์มหาวิทยาลัย
ปีการศึกษา 2561

Thesis Title	Thermal stability characterization of tunneling magneto resistive structure for data storage applications
By	Mr. Pornchai Rakpongsiri
Field of Study	Nanoscience and Technology
Thesis Advisor	Assistant Professor Sukkaneste Tungasmita, Ph.D.
Thesis Co Advisor	Kurt Ruthe, Ph.D.

Accepted by the Graduate School, Chulalongkorn University in Partial Fulfillment of the Requirement for the Doctor of Philosophy

.... Dean of the Graduate School
(Associate Professor THUMNOON NHUJAK, Ph.D.)

DISSERTATION COMMITTEE

.... Chairman
(Associate Professor Vudhichai Parasuk, Ph.D.)

.... Thesis Advisor
(Assistant Professor Sukkaneste Tungasmita, Ph.D.)

.... Thesis Co-Advisor
(Kurt Ruthe, Ph.D.)

.... Examiner
(Associate Professor SAKUNTAM SANORPIM, Ph.D.)

.... Examiner
(Assistant Professor RATTHAPOL RANGKUPAN, Ph.D.)

.... External Examiner
(Duangporn Sompongse, Ph.D.)

พรชัย รักษ์พงษ์สิริ : การวิเคราะห์ความเสถียรเชิงความร้อนของโครงสร้างแบบทันเนอริงแมกนิโตรีซิสทิฟเพื่อประยุกต์ใช้งานด้านการเก็บข้อมูล. (Thermal stability characterization of tunneling magneto resistive structure for data storage applications) อ.ที่ปรึกษาหลัก : ผศ. ดร.สุคคเณศ ตุงคะสมิต, อ.ที่ปรึกษาร่วม : ดร.เคริท รูเธอร์

เทคโนโลยีปัจจุบันของตัวอ่านข้อมูลบันทึกแถบแม่เหล็กในฮาร์ดิสไดร์คือ ทันเนอริงแมกนิโตรีซิสทิฟ ซึ่งวิวัฒนาการเทคโนโลยีนี้ได้รับการพัฒนาอย่างต่อเนื่องเพื่อให้มีความสามารถขั้นสูงในขั้นตอนการอ่านข้อมูลบันทึกสนามแม่เหล็กขนาดเล็กอย่างมีประสิทธิภาพ อันส่งผลให้โครงสร้างของทันเนอริงแมกนิโตรีซิสทิฟมีความบอบบางและซับซ้อนซึ่งยังผลให้มีความไวต่อการเสื่อมประสิทธิภาพอันเนื่องจากความร้อนหรือข้อบกพร่องเพียงเล็กน้อยในโครงสร้าง ในการทดลองนี้ได้ใช้ความร้อนที่อุณหภูมิระหว่าง 150-250 ^{o}C ทำการศึกษาสเถียรภาพของทันเนอริงแมกนิโตรีซิสทิฟ โดยได้มีการวัดค่า ความต้านทาน แอมพลิจูด และความสมมาตรของสัญญาน ทั้งก่อนและหลังการกระตุ้นเพื่อสังเกตการเปลี่ยนแปลงของโครงสร้างที่สามารถตรวจจับได้จากเครื่องวัด quasi-static tester (QST) จากผลการทดลองแสดงให้เห็นอุณหภูมิในการกระตุ้นมีความสัมพันธ์ต่อเปอร์เซ็นการเปลี่ยนแปลงค่าความต้านทาน แอมพลิจูด และความสมมาตรของสัญญาน ในการวิเคราะห์โครงสร้างระดับนาโนของทันเนอริงแมกนิโตรีซิสทิฟที่ผ่านการกระตุ้นด้วยความร้อนโดยใช้เครื่องมือ TEM, STEM and XEDS พบว่าโครงสร้างที่บกพร่องนั้นสอดคล้องกับค่าการเปลี่ยนแปลงของ QST parametric ทั้งการบิดเบี้ยวในการเรียงตัวของชั้น MgO และการหายไปของอะตอม Mn นั้น ส่งผลให้เกิดความไม่เสถียรของการตอบสนองทางแม่เหล็กหลังจากการกระตุ้นด้วยความร้อนสูง การศึกษาให้ความร้อนด้วยอุปกรณ์ที่ติดตั้งภายในเครื่อง STEM ซึ่งสามารถสังเกตการเปลี่ยนแปลงได้ตลอดเวลานั้น พบลักษณะคล้ายมีการเปลี่ยนแปลงของชั้น Ru ที่อุณหภูมิ 350 ^{o}C ซึ่งบ่งบอกว่าสารที่มีน้ำหนักอะตอมที่น้อยกว่า Ru นั้นได้เกิดการกระจายตัวไปยังชั้นต่าง ๆ ของสารที่อยู่ติดกันด้วย และผลของการกระตุ้นด้วยเลเซอร์นั้นก็ได้สังเกตเห็นการลดลงของแอมพลิจูดโดยไม่เห็นถึงการเปลี่ยนแปลงของค่าความต้านทานหรือความสมมาตรของสัญญาน ส่วนผลการวิเคราะห์ STEM และ XEDS บ่งชี้ว่ามีการหายไปของ Mn บางส่วนในชั้นของ antiferromagnetic

สาขาวิชา วิทยาศาสตร์นาโนและเทคโนโลยี
ปีการศึกษา 2561

ลายมือชื่อนิสิต ....
ลายมือชื่อ อ.ที่ปรึกษาหลัก ....
ลายมือชื่อ อ.ที่ปรึกษาร่วม ....

5787793420 : MAJOR NANOSCIENCE AND TECHNOLOGY

KEYWORD: Tunneling magnetoresistive, Degradation, Thermal induced

Pornchai Rakpongsiri : Thermal stability characterization of tunneling magneto resistive structure for data storage applications. Advisor: Asst. Prof. Sukkaneste Tungasmita, Ph.D. Co-advisor: Kurt Ruthe, Ph.D.

The conventional read sensor technology used in hard disk drives is the tunneling magneto resistive (TMR) device. The revolutions of technology have been developed to achieve high performance of reading signal resulting in very thin and complicated device layers which thermal induced degradation and defects would be concerned. In this research, a thermal stress has been applied to TMR devices between 150-250 °C for reliability investigation. The resistance, amplitude and asymmetry parameters, before and after the thermal stress, were measured using a quasi-static tester (QST). The results showed the temperature dependence of the percentage change in QST resistance, asymmetry and amplitude. The microstructure of the annealed devices was observed using TEM, STEM and XEDS. It was found that structural defects that can be related to the QST parametric changes. Both atomic misalignment of MgO layer and Mn depletion can lead to instability of the magnetic response of TMR after be stressed at high temperature. The *in-situ* real-time annealing STEM showed a sign of Ru interface change at 350 ^{o}C which lower atomic weight elements can diffuse to adjacent layers. The laser stress results exhibit amplitude degradation without changing in resistance and asymmetry. STEM and XEDS analysis indicate portion of Mn depletion in antiferromagnetic layer.

Field of Study:	Nanoscience and Technology	Student's Signature ....
Academic Year:	2018	Advisor's Signature ....
		Co-advisor's Signature ....

ACKNOWLEDGEMENTS

The authors would like to thank Western Digital (Thailand) Co., Ltd. and Chulalongkorn University for all the supports. The authors also would like to thank the Knut and Alice Wallenberg foundation for support of the electron microscopy laboratory in Linköping. The Swedish Research Council (VR) under grant 2016-04412 as well as the Swedish Government Strategic Research Area in Materials Science on Functional Materials at Linköping University (Faculty Grant SFO-Mat-LiU 2009-00971) is finally acknowledged for financial support.

Pornchai Rakpongsiri

TABLE OF CONTENTS

Page

List of Figures

List of Tables

CHAPTER I

INTRODUCTION

1.1 Overview and motivation

In hard disk drive for storage, the major components compose of magnetic spinning disks and write/read heads which shows in Fig. 1.1. The digital data signal of computer are recorded on the magnetic disk in the form of submicron magnets aligned in the *north pole* (N) or *south pole* (S) directions, depending on “0” or “1” data signal. These recorded submicron magnets are called “data bits”(1).

Fig. 1.1. Hard drive components and write/read heads (1).

The transformation of the digital data signal to the magnetic bits is called “writing process”. This process is done by using magnetic induction method via the copper coils turning around the soft magnetic core structure to magnetize the magnetic thin film on the spinning magnetic-disk (1).

The data writing technology in HDD has been started from *longitudinal magnetic recording* (LMR), later changed to *perpendicular magnetic recording* (PMR) in order to achieve higher linear bit density. With the requirement of higher aerials density, the writing technologies have to develop the capability technique to write the very small and weak magnetic field on the high coercivity media.In the near future, the *heat assistance magnetic recording* (HAMR) technologies are developing for the next generation. The modern HAMR technology uses laser beam to warm up the media for reducing the magnetic coercivity (H_c) which help weak writing magnetic flux able to record the data on the high coercivity media material successfully. Another potential option for energy assistance is *microwave assistance magnetic recording* (MAMR) for activating the magnetic domains of media to unstable states for helping the writing process capable to record the data onto the high coercivity media. Other technologies are also put in the roadmap such as *shingle write recording* (SMR), *two dimensional magnetic recording* (TDMR) and *bit patterned magnetic recording* (BPMR), see in Fig. 1.2.

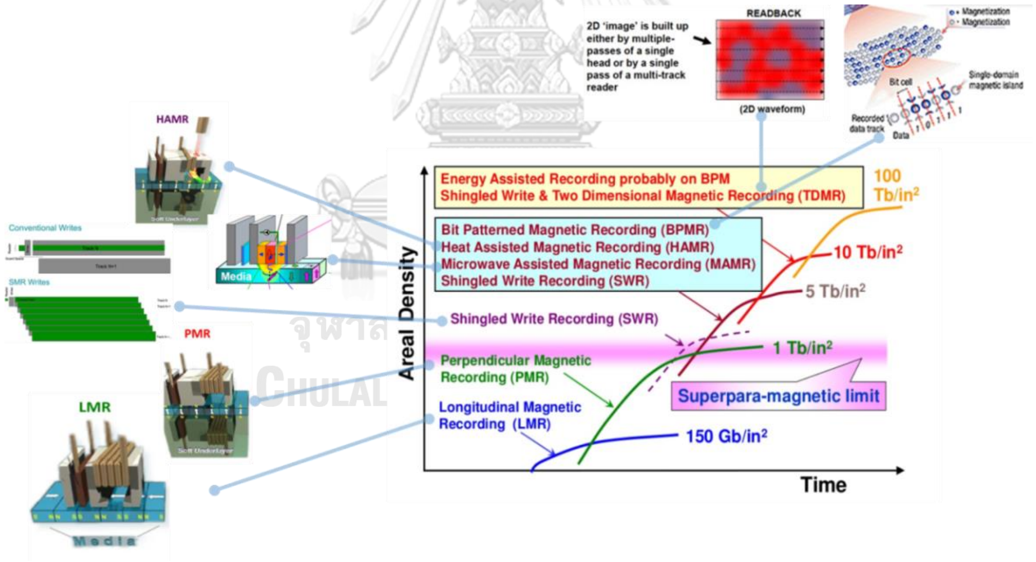

Fig. 1.2. Magnetic recording technology roadmap (2).

For "reading process", it started from using induction method for reading back the data from the disk by using the same structure of writing structure. Later, the magnetic bit size had been dramatically reduced to achieve the extremely high areal density per market requirement, then it had problem of very weak read back signal, and caused poor *signal-to-noise ratio* (SNR). Then the *anisotropic magneto resistive* (AMR) reader sensor technology had been introduced to step over the problem. The AMR reader element was placed close to the writer structure for sensing the magnetic data bits. However, the higher areal density requirement keeps going, and reaching the point that the AMR sensor was not effective, then better sensitivity magnetic reader technologies as *giant magneto resistive* (GMR) and *tunneling magneto resistive* (TMR) sensors have been applied, respectively (2, 3).

The TMR device structure composes of free layer, barrier, pinned layer and pinning layer. In general, the free layer and pinned layer are made of soft magnetic materials such as NiFe or NiFeB, and the pinning layer is made of antiferromagnetic materials such as IrMn or PtMn. The insulator materials for spacer layer are MgO and AlOx to induce magnetic tunneling effect as show in Fig. 1.3 (4, 5).

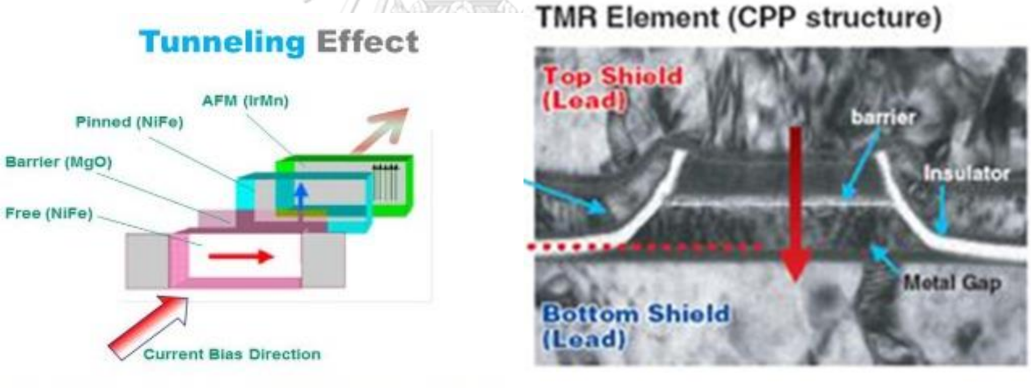

(a) (b)

Fig. 1.3. TMR structure; (a) Schematic of TMR and (b) TEM picture of TMR (5, 6).

The TMR device has resistance change property according to the applied magnetic field. The changes of resistance are related to the relative angle between the magnetization direction of free layer and pinned layer. As the free layer magnetization direction is in parallel with the pinned layer, the electrons easily pass through the interface layers and give low resistance, but if the magnetization direction of free layer is in the opposite direction to the pinned later, the electrons difficulty pass the interface layers, and give high resistance. For magnetic recording data sensing function, the devices have been designed the free layer moving freely when the pinned later is fixed via magnetic coupling of antiferromagnetic layer (5, 6).

In manufacturing, the *quasi static tester* (QST) is commonly used for testing the reader response to verify good or bad devices. The dc bias is applied to the reader for measuring the resistance change due to external electromagnetic field to simulate the field of magnetic data bit. The fundamental measurement parameters are; (1) MRR (static resistance of the reader under zero magnetic field), (2) *amplitude* (peak to peak voltage measured from the reader resistance change due to the apply magnetic field under dc current bias), (3) *asymmetry* (calculated symmetry of amplitude response for positive and negative magnetic field), (4) *bark jump* (jumping signal due to unstable of magnetic domain) (7).

Even though the technologies of magnetic recording will have big changes, however in general of hard drive manufacturing processes, there are not much changed. There are five major processes steps have been classified for flexibility manufacturing management which compose of wafer fabrication, slider fabrication, head gimbal assembly, head stack assembly and hard disk drive assembly, as shows in Fig. 1.4 (8).

Fig. 1.4. Hard drive assembly process flow in general (8).

The TMR reader revolutions have to be designed with reducing the dimensions to accurately read the smaller magnetic data bit per higher areal density requirement. The reader width needed to be reduced to avoid the interference of magnetic field from the adjacent magnetic data bits. The reader thickness is required thinner to have smaller shield to shield spacing for supporting the shorter inline magnetic data bit length. The reader stripe height is reduced to optimize the current bias and effective magnetic sensing properties. With the constrain of smaller TMR volumes, the sensor needed to be designed with more complex of multilayers and thinner layers to keep the effective sensitivity of reading signal (8).

The TMR device is fabricated with high resolution photolithography and multilayer thin film deposition. The wafers also passed through slider (read/write head) fabrication for lapping to achieve precise dimensions in the nanometer scale before the HDD assembly processes. Due to the very thin and complex multi-layered structure of the TMR device in HDD head, reliability is a concern, and drive operational failure may occur due to degradation of the layers and interfaces of the TMR structure (9, 10). Thermal, mechanical, and electrical stresses may all contribute to the failure of the device. As tunneling through the insulating barrier in the TMR device is a thermally activated process, thermal stress is considered to be a significant factor causing TMR device degradation. Such stresses can be originated not only from the high temperatures used in the manufacturing processes such as magnetic annealing, epoxy-curing process, electrostatic discharge and thermal stress during reliability tests, but also the thermal effects of dynamic-fly-height (DFH) element during operation (11-14).

To understand and investigate the influence of thermal stress on TMR structure degradation and interface defects within the temperature range of the fabrication processes and drive operation is important for improving the HDD process and device design that could resist to the thermal degradation which help prevent the degradation of performance and poor reliability. In additional, laser stress on the TMR also be studies since the application of laser diode in HAMR in future technology might cause side effect of degradation on TMR.

1.2 Objectives

1. Understanding fundamental of the commercial TMR structure degradation and cause of defect due to thermal stress
2. Understand the fundamental of the physical changes in the TMR microstructure that result on the TMR response changes
3. Apply the knowledge for failure analysis and manufacturing process improvement

1.3 Scope of research

The study has been separated into three parts ;

Part 1. ***Thermal stress study by using heater module annealing***

The magnetic-heads were measured the magnetic properties by Quasi Static Test (QST), and stress with the thermal module at 25, 150, 200, 225 and 250 ^{o}C, 30 minutes for each group. Then re-measure QST again after the stress, and calculate the parametric change to verify the device degradation. Microstructural analysis of the device layers was employed in order to investigate what physical changes in the device might explain the degradation of performance and reliabilfity.

Part 2. ***Thermal stress study by using in-situ annealing equip with TEM***

The magnetic-head has been prepared by using FIB, and loaded on the heat source fixture which was built-in the TEM machine. The sample was taken the TEM image in real time during thermally stress on the device. Starting temperature from 25 ^{o}C, then increasing to 150 ^{o}C, 250 ^{o}C and 350 ^{o}C. Each step the thermal stress was 30 minutes

Part 3. ***Thermal stress study by using laser excitation***

The magnetic-heads were measured the magnetic properties by Quasi Static Test (QST), and stress with laser 10 seconds each head, then re-measure QST again after the stress. After repeat 20 cycles, then calculate the parametric change to verify the device degradation. Microstructural analysis of the device layers was employed in order to investigate what physical changes in the device might explain the degradation of performance and reliability.

CHAPTER II

THEORY AND LITERATURE REVIEW

2.1 Tunneling magneto resistance (TMR)

In general, the current cannot flow through the insulator. However, for the very thin insulator in the scale of few angstroms, the current could penetrate by ballistic transport (15). When the very thin insulator is sandwiched with soft magnetic materials that could cause the spin polarized current flow through the layer as a result of TMR effect. The magnitude of TMR depends on the relative magnetization angle between the two of soft magnetic layers. The TMR magnetic thin film is normally used in magnetic data storage. Others applications are spin filter (15), semimetal materials (16) and ferroelectric (17).

The *TMR effect* was discovered by Julliere in 1975 with 14% TMR ratio which was observed in the structure of Fe/Ge/Co at 4.3 K (18). The effect is spin-dependent scattering of electrons tunneling through the thin insulator that was sandwiched with two ferromagnetic materials. For better understanding, I would like to describe how this phenomenal behave with solid state physics, and to explain what would concern the properties of TMR characteristic.

The early TMR thin film device was fabricated by Miyazaki and Moodera (19, 20). The Al-O barrier was used in the prototype magnetic head in 2002 (21), and the 150 Gbit/inch^2 areal density product was reported in 2004 (22). In 2006, the TMR has been commercially used for 300 Gbit/inch^2 (8). Butter had studied the electronic structure of TMR thin film with MgO barrier, and the calculation result showed the TMR ration was about 1,000% (23). By this calculation concept, in 2004 S.S.P. Parkin (24) and Yuasa (25) had successes the fabrication of the magnetic thin file TMR with MgO barrier which was sandwiched with CoFeB magnetic thin film layers, and gave TMR ratio about 230% (26). This structure has been wildly used in magnetic data recording application until today. The TMR technology has been developed for more efficient to support extremely high areal density requirement.

The basic structure of TMR composes of two *ferromagnetic layers*; a *free layer* (FL) and a *pinned layer* (PL). The two ferromagnetic layers are separated by very thin insulator, called "*barrier layer"* (see Fig. 2.1).The magnetization of free layer could be moved freely when the pinned layer magnetization was fixed. The external magnetic field could induce and change the free layer magnetization direction which cause relative magnetization angle between free and pinned layers change as a result of changing the *magnetoresistance*. If the magnetization direction of free and pinned layers are in parallel, the current could go through the device easily, and be called *parallel condition current* (I_P) and given *low resistance condition*. On the other hand, if the magnetization of free and pinned layers are in opposite direction, the current is difficulty to pass the device, and be called *antiparallel condition current* (I_{AP}) and given *high resistance condition*. So, the TMR ratio can be written as (2.1) (27).

$$\text{TMR Ratio} = \frac{I_P - I_{AP}}{I_{AP}} \qquad (2.1)$$

And it can be written in the resistance form as (2.2) [28].

$$\text{TMR Ratio} = \frac{R_{AP} - R_P}{R_P} \qquad (2.2)$$

Where ;

$\boldsymbol{R_{AP}}$: Antiparallel condition resistance

$\boldsymbol{R_P}$: Parallel condition resistance

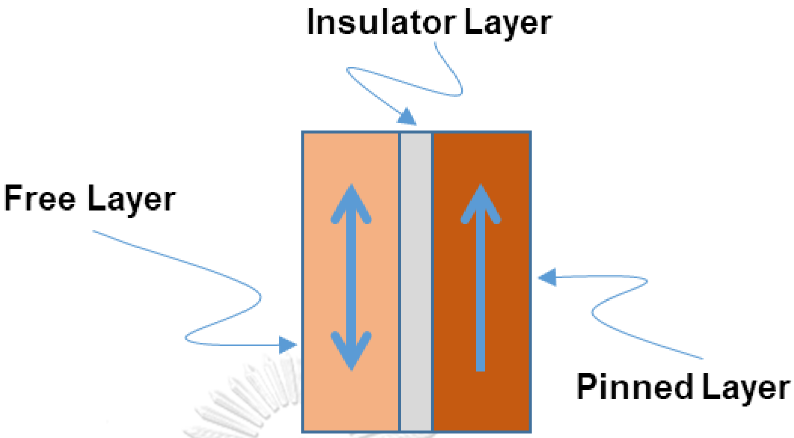

Fig. 2.1 Basic concept structure of magnetic thin film TMR

TMR effect could be explained by using *Jullier model* which has been proposed in 1975 (28). Jullier used DOS to explain the number of *up-spin* and *down-spin* electrons transferring between two magnetic material layers from the left to the right by passing through the thin insulator. His assumptions are; (1) spin direction will not be changed when passing through the insulator layer, and (2) electrons that pass the insulator layer will be moved to the zone that has the same spin condition. The up-spin electrons will be moved to up-spin zone, and the down-spin electrons will be moved to the down-spin zone.

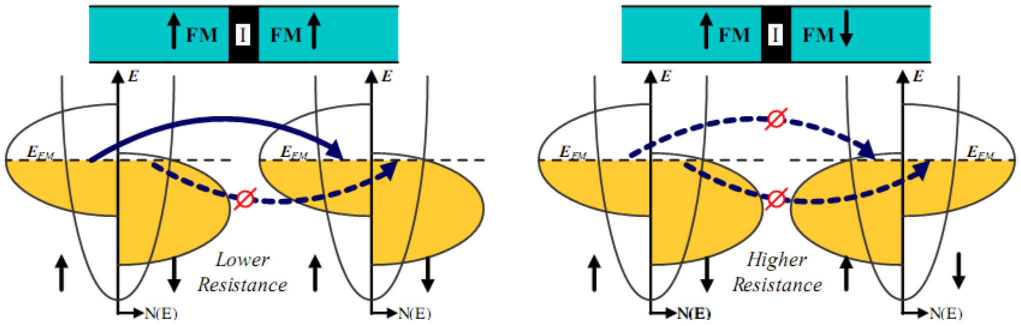

(a) (b)

Fig. 2.2 Diagram of DOS and polarization; (a) Magnetization of ferromagnetic material in parallel condition, and (b) Magnetization of ferromagnetic material in antiparallel (29).

From Fig. 2.2 (a), the magnetization of ferromagnetic layers is in *parallel condition*. If we consider the up-spin electrons, the DOS at Fermi level is high for the transmit-side which means high number of up-spin electrons that could be transported. For the receive-side, the DOS is also high which means it could receive high number of up-spin electrons. So, the current of up-spin electron is high in this condition. For the down-spin, both transmit-side and receive-side have low values of the DOS which means the current from down-spin electrons transportation is low. So, the overall current is high, as a result of low resistance of TMR. The current on TMR in parallel condition could be written as (2.3) (30).

$$I_P \propto N_{\uparrow}^{L} N_{\uparrow}^{R} + N_{\downarrow}^{L} N_{\downarrow}^{R} \tag{2.3}$$

Where;

I_P : Current in parallel condition

$N_{\uparrow(\downarrow)}^{L\ (R)}$: Number of up-spin and down-spin electrons on the left and the right electrodes

From Fig. 2.2 (b), the magnetization of ferromagnetic layers is in *antiparallel condition*. The DOS of up-spin on the transmit-side is high, but the DOS on the receive-side is low. So, the current from up-spin electrons is also low. For the down-spin, the DOS is low on the transmit-side as a result of low current even through the DOS is high on the receive-side. So, the overall current is low in antiparallel condition, as a result of high resistance of TMR. The current of antiparallel condition TMR could be written as (2.4) (30).

$$\mathrm{I}_{\mathrm{AP}} \propto \mathrm{N}_{\uparrow}^{L}\mathrm{N}_{\downarrow}^{R} + \mathrm{N}_{\downarrow}^{L}\mathrm{N}_{\uparrow}^{R} \qquad (2.4)$$

Where;

$\mathbf{I_{AP}}$: Current in antiparallel condition

$\mathrm{N}_{\uparrow(\downarrow)}^{L\ (R)}$: Number of up-spin and down-spin electrons on the left and the right electrodes

Put $\mathrm{I_P}$ and $\mathrm{I_{AP}}$ in (2.1), then we can get TMR ratio in the form of spin polarization (30) as in (2.5).

$$\text{TMR Ratio} = \frac{2P_L P_R}{1-P_L P_R} \qquad (2.5)$$

Where; **P** is *spin polarization,* calculated from $\mathrm{P}_i = \dfrac{N_{\uparrow}^{i} - N_{\downarrow}^{i}}{N_{\uparrow}^{i} + N_{\downarrow}^{i}}$

From (2.5), if we need higher TMR ratio, we have to select materials with high **P**. The CoFeB can give very high **P** about 65% (31), as the materials are currently used in magnetic data recording that can give very high TMR ratio.

The *symmetry* of *wave function* is also important factor for improving efficiency of the thin film TMR because it relates to the *reduction rate of electron spinning* (32). In quantum mechanics, electrons have wave function property. So, when they go through the insulator region, the energy levels reduce exponentially, and called “*decay rate*”. The decay rate relates to *decay factor*. For crystalize structure insulator, the decay relates to wave function and thickness of the material (33) as shows in (2.6).

$$T \propto \exp(-2k^{\sigma}d) \qquad (2.6)$$

Where :

T = Decay rate of wave function

k = ***k*** index

d = Thickness of insulator

σ = Spin condition

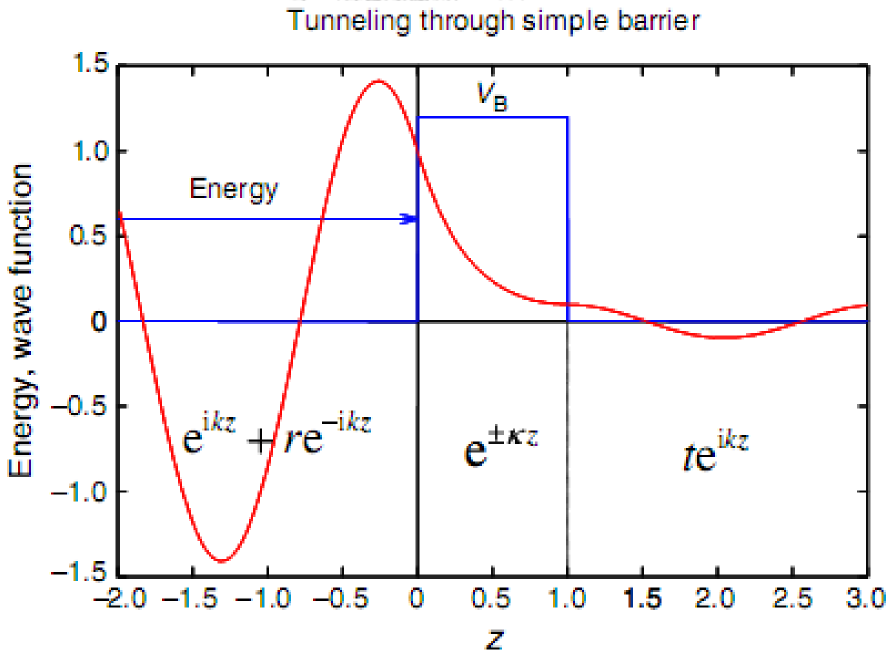

Fig. 2.3 Show the incident electrons wave function ($e^{ikz}+re^{-ikz}$), the transmitted electrons wave function (te^{-ikz}), and the electron weave function decay in the insulator region ($e^{\pm kz}$) (32).

From Fig. 2.3, the *decay rate* of electron wave function in the crystal region relates to reduction of spin electrons. When the spin electrons flow to the *evanescence state* of insulator layer, the decay rate would relate to *wave function symmetry*. And the symmetry of the wave function could be found in *symmetry of crystal structure* such as MgO. In amorphous materials, the wave function symmetry property could not be observed (33, 34), see Fig. 2.4.

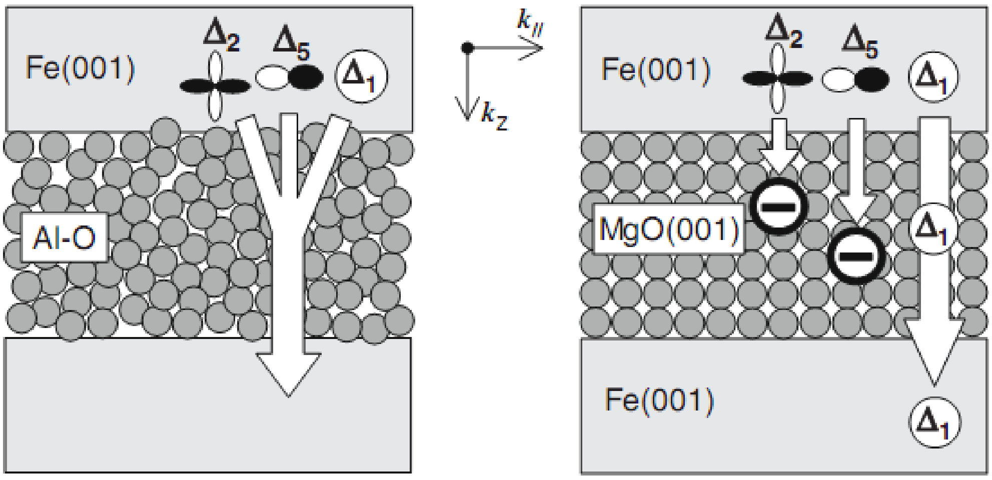

(a) (b)

Fig. 2.4 Electron transportation diagram for Al-O and MgO insulator in thin film TMR (33, 34); (a) Electron transport in Al-O amorphous thin film, no wave function symmetry. (b) Electron transport in thin film MgO crystal structure, with wave function symmetry.

The symmetry of wave function has been classified by *symmetry of electrons distribution* of individual atomic orbital. There are 4 types of symmetry (33, 34); (1) Δ_1 is symmetry of electrons distribution in orbital *s*, (2) Δ_5 is symmetry of electrons distribution in orbital p_x, p_y, d_{xz} and d_{yz}, the symmetry of Δ_5 is majority in *d* orbital, (3) Δ_2 is a symmetry of electrons distribution in orbital $d_{x^2-y^2}$, and (4) $\Delta_{2'}$ is a symmetry of electrons distribution in orbital d_{xy}.

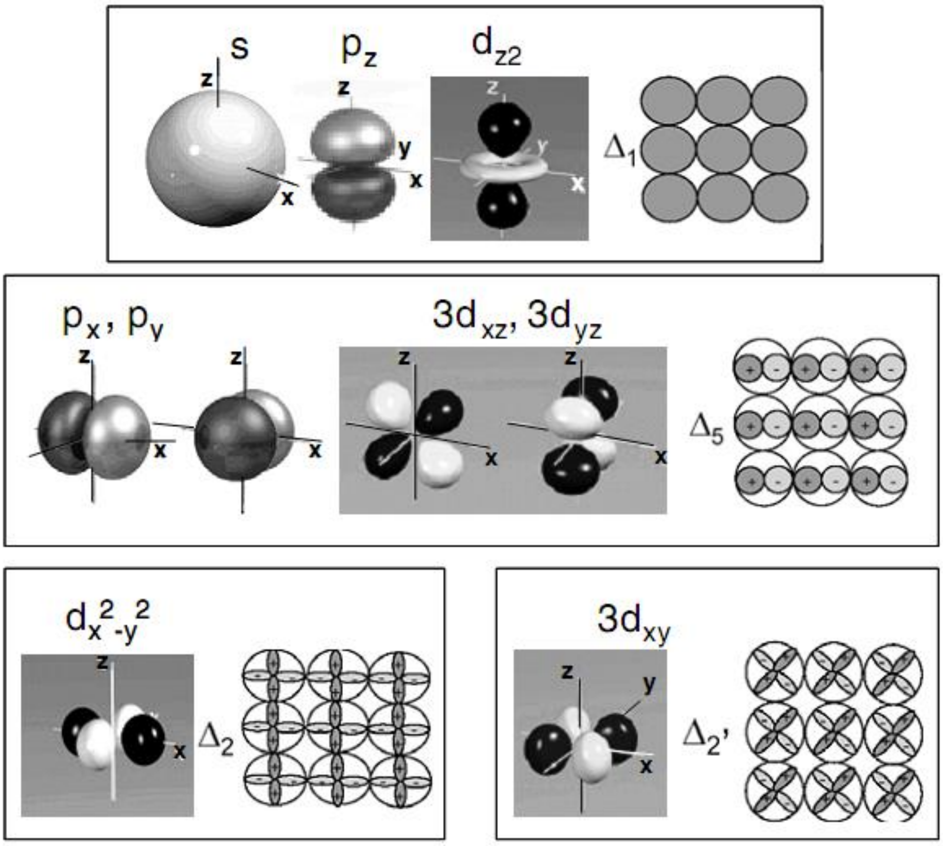

Fig. 2.5 Types of symmetry and Atomic Orbital (33).

From Fig. 2.5, when we consider the *nodes* that link in crystal structure, Δ_1 has bigger symmetry than Δ_5, Δ_2 and $\Delta_{2'}$ respectively. So, in a crystal, the numbers of node that link in the symmetry Δ_1 are lower than the number of node of symmetry Δ_5, Δ_2 และ $\Delta_{2'}$ respectively, as a result of the decay rate of symmetry Δ_1 is lower than the decay rate of symmetry Δ_5, Δ_2 and $\Delta_{2'}$ respectively. So, the spin electrons passing through the evanescence state of symmetry Δ_1 will be less decayed than passing through symmetry Δ_5 Δ_2 and $\Delta_{2'}$ respectively, as a result of higher TMR ratio.

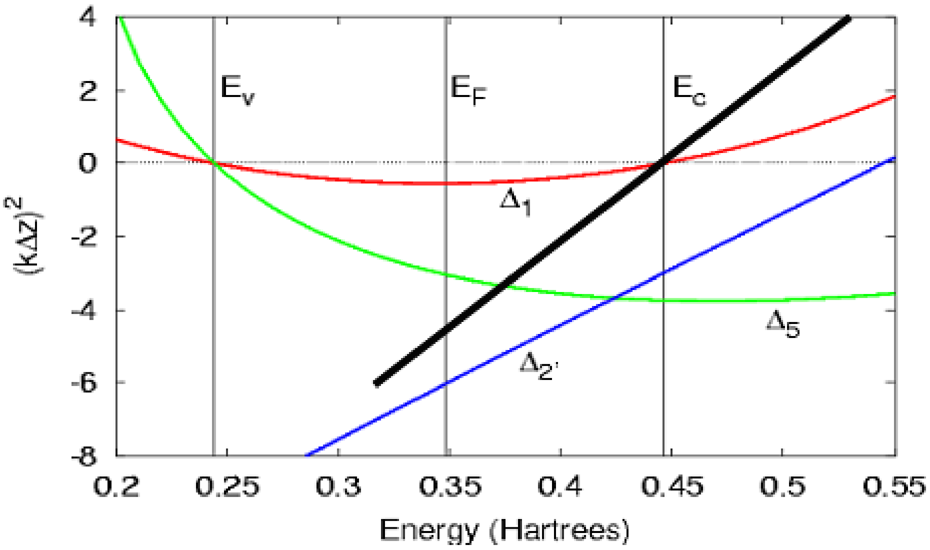

Fig. 2.6 Relation of energy and $(k\Delta z)^2$. Only the line $(k\Delta z)^2$ of symmetry Δ_1 has continuity from *valence zone*, passing evanescence zone of insulator to the *conduction zone* (32).

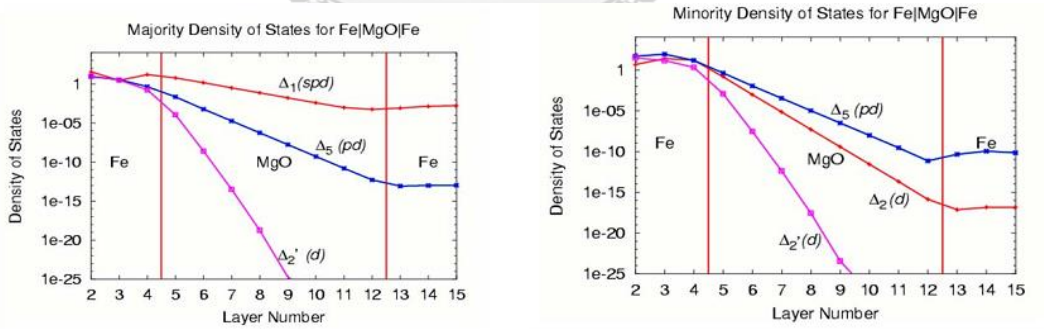

(a) (b)

Fig. 2.7 Example calculation of DOS of Fe/MgO/Fe structure (32); (a) up-spin electron on both electrodes, and (b) down-spin electron on both electrodes.

Fig. 2.6 shows decay rate symmetry types of MgO material. $(k\Delta z)^2$ is *momentum property* of *complex band structure*. The negative values of $(k\Delta z)^2$ shows degree of decay, $\mathbf{E_v}$ is *valence band energy level*, and $\mathbf{E_c}$ is *conduction band energy level*. We could observe that on the valence band have symmetry Δ_1 and $\Delta_{5,}$ when on the conduction band only symmetry Δ_1 is available. In general, the fabrication of ferromagnetic material on insulator layer, the symmetry of spin-electron that penetrate the insulator layer will not be changed the symmetry, the symmetry of spin is continuous with the symmetry in the evanescence state of insulator. In case of up-spin, the Fermi energy level has symmetry Δ_1, higher than others symmetry. But in case of down-spin, the symmetry Δ_1 is not observed, as a result of very high magneto resistive TMR ratio.

Fig. 2.7 shows the calculation result of the DOS of electrons flow from Fe, passing through MgO, then to Fe on another side. In case of up-spin, symmetry Δ_1 has less decay than others symmetry, which means the number of up-spin electron passing through insulator is slightly changed. In case of down-spin, there is no symmetry Δ_1, and the down-spin cannot pass the insulator. That means the symmetry Δ_1 has the spin filter property, only up-spin electrons are allowed passing through, but down-spin electrons are not allowed. With this property, the TMR with Fe-MgO-Fe structure has high ratio TMR about 1000% . TMR thin film with Fe electrodes and MgO barrier has been first fabricated in 2007. However, in magnetic recording, we use CoFeB for free and pinned layers, and use MgO for barrier. The barrier usually made of AlO and MgO (5). The AlO layer is amorphous which causes the tunneling electrons be scattered, as a result of low TMR ratio. So, the MgO is preferable because of crystallization property. With the good atomic orientation in the crystalize structure, the electrons transport has no effect of scattering in the perfect crystal, and give very high TMR ratio (35). In wafer fabrication process, the crystalline layer deposition of MgO sandwiched with two ferromagnetic materials are very importance. The ferromagnetic layers such as Co or Fe or their alloys are preferred to have interfacing to the MgO layer on (001) plan to minimize lattice mismatch which would help reduce electron scattering problem (36, 37).

The ferromagnetic layer has the *face center cubic* (FCC) structure, while the MgO barrier layer has the *body center cubic* (BCC) structure. So, to deposit MgO layer on the ferromagnetic layer is difficult to make the epitaxial crystallization structure because of different atomic structure. D. D. Djayaprawira et. al. had studied the CoFeB/MgO/CoFeB TMR structure. In their experiment, they found very high TMR ratio at about 230% - 290% compared to the previous reported at that time about 62% for the structure of CoFe-reference layer and CoFe/NiFe-free layer. In the analysis with *high resolution transmission microscope* (HRTEM), they surprisingly observed the MgO (001) crystallization was grown on the amorphous of CoFeB layer with very clear interface of the lower and the upper layers. They believed the very high MR ratio could be achieved from the high crystalize quality of MgQ barrier that was sandwiched with the two amorphous ferromagnetic electrodes. This finding is to explain the symmetry of MgO (001) barrier is the critical factor to obtain high MR ratio, which is essential for coherent spin-polarized tunneling of Δ_1 electrons (37). Later, Yuasa S et. al. had studied the growth mechanism by using *in situ reflective high-energy electron diffraction* (RHEED) (38). They found that, the MgO film had started from amorphous phase, then become crystallize (001) preferred plane after the thickness higher than 1.0 nm. They also reported that, the annealing process at 250^{o}C, the $Co_{60}Fe_{20}B_{20}$ amorphous layers were transformed to BCC crystallization structure because of MgO (001) layer influencing, although the thermodynamically stable crystal structure of $Co_{60}Fe_{20}B_{20}$ was FCC (39). With this finding, the technique could be developed to fabricate the CoFeB/MgO/CoFeB to be single crystalize structure in (001) plane to minimize electrons scattering which could enhance the TMR ratio.

Tsunekawa et. Al. had studied the effect of deposition material on top of CoFeB layer, which was called ***"cap layer"***. They experimented by using various materials, such as NiFe, Ru and Ta (40). They found that a Ru and Ta cap layer did not show the effect on the CoFeB electrode but $Ni_{0.8}Fe_{0.2}$ (permalloy) showed significantly affecting on the CoFeB crystallization after the annealing at 200^{o}C. When the annealing temperature increased up to 250^{o}C, the CoFeB which was FCC stable structure did not change to BCC structure to match with MgO layer. So, the Ru or Ta are generally used for cap layer.

The TMR ratio also depends on the *composition* and the *thicknesses* of the CoFeB film. Lee Y. M. reported that the TMR structure with a 4 nm thickness $(Co_{25}Fe_{75})_{80}B_{20}$ electrodes and a 2.1nm thickness of MgO barrier layer, annealed at 475 °C, was 500% at room temperature (300 K), and could be up to 1010% at 5 K temperature (41).

In the application of TMR device, the pin layer needs to be fixed the magnetization direction in order to sense the external field via the changing of the free layer magnetization only. The *pinned layer* is sometime called *"reference layer"*. To fix the pinned layer could be used *permanent magnetic* or *antiferromagnetic* to coupling the pinned layer. However, the antiferromagnetic coupling is generally used because it doesn't have the effect of expose field to interfere the reading signal. The selected antiferromagnetic material needs to be considered; (1) *high magnetic coupling exchange* to strengthen the pinned layer in the fixed direction, (2) *high blocking temperature* to resist the high temperature from manufacturing process and internal heater element, and (3) *low critical thickness* to minimize shield to shield spacing which is very critical parameter for high areal density head design.

Antiferromagnetic materials such as IrMn, PtMn, FeMn and NiMn have been study the properties, and found that IrMn is the good candidate for magnetic data storage application due to it has the lowest critical thickness (7-8 Å) when it has high exchange field (400 Oe) and high blocking temperature (250 ^{o}C) as shows in Table 1 (42, 43).

Table 2.1 Antiferromagnetic materials and properties (42, 43).

AFM material	***IrMn***	***PtMn***	***FeMn***	***NiMn***
Exchange bias field (Oe)	400	500	420	450
Blocking temperature (^{o}C)	250	350	150	370
Critical thickness (nm)	7-8	10-15	7-10	25

The ratio between Ir and Mn has been studies, and found 80% – 85% of Mn would give the highest exchange magnetic field property as shows in Fig. 2.8 (44). So, the controlling ratio of Ir and Mn is critical to achieve the high coupling field to the pinned layer as a result of good stability of the device. The depletion of Ir or Mn due to any reason could cause weak magnetic coupling field, and affect poor fixing function to the pinned magnetization, that might cause spike signal due to multi domains have been formed on pinned layer which is called *"Barkhausen Jump"*.

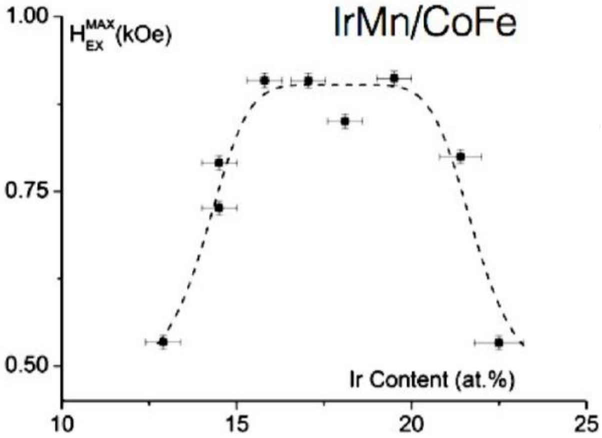

Fig. 2.8 IrMn composition and magnetic coupling field (44).

As the lower shield to shield spacing is critical for improving the *down track* for high data *bit per inch* (BPI) in order to improve the resolution to verify the very high density packing magnetic data bits in the linear direction, so the minimum thickness of the TMR component layers are required. The possible thinnest of IrMn that still keep antiferromagnetic property is about 7-8 nm as shows in Fig. 2.9 (45), and it is the most thinnest among others antiferromagnetic materials.

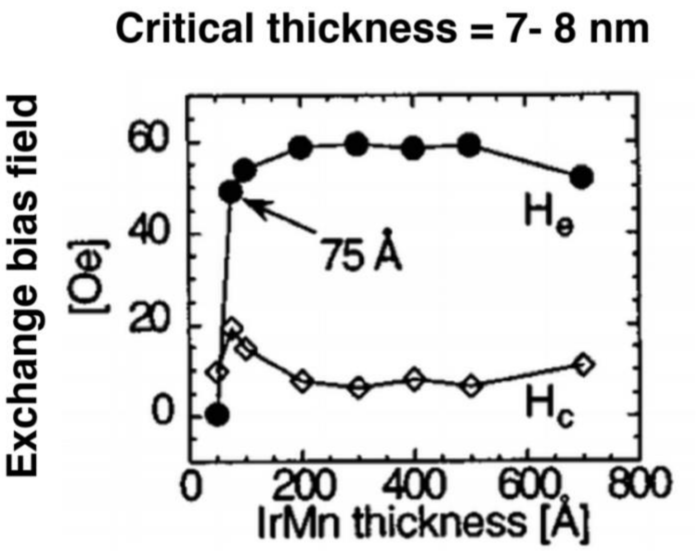

Fig. 2.9 IrMn thin film thickness and exchange coupling field, critical thickness is about 7-8 nm (45).

Annealing the magnetic thin film is a way to help improve the exchange field property due to more crystalized structure atomic arrangement. We could observe the higher intensity x-ray diffraction after annealing that compares to as-deposited peaks as shows in Fig. 2.10. The increasing peak intensity could be explained that the growth of more crystalized structure atomic arrangement (46).

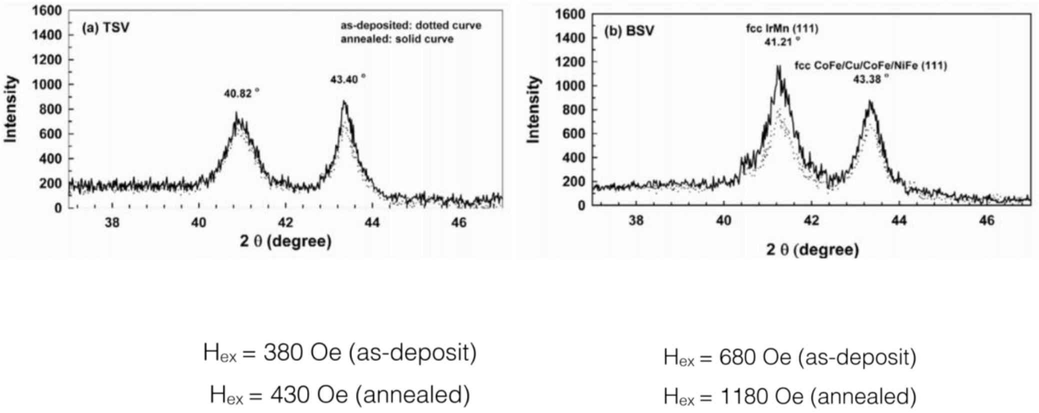

Fig. 2.10 Annealing magnetic thin film study for helping crystallization atomic structure and improving exchange magnetic field (46).

2.2 Magnetic noise of TMR

One of noise source on TMR is happened from *Barkhausen effect* which is a noise of ferromagnetic materials. This effect was discovered by German physicist *Heinrich Barkhausen* in 1991, it is an effect from rapidly changing the magnetic domain size or the moving of domain wall.

He worked in acoustics and magnetism, and his discovery became a major finding evident supporting the *domain theory* of ferromagnetic that *Pierre-Ernest Weiss* was proposed in 1906 (47).

The *Bakhausen effect* is a suddenly change in the size and orientation of ferromagnetic domains. In the microscopic, it is a change of atomic magnetic cluster aliment or spins. This occurs during a continuous process of magnetization or demagnetization. The *Barkhausen effect* is the evidence that confirms the existence of ferromagnetic domains, which had been postulated theoretically before. He found that a slow and smooth increase of an applied magnetic field to ferromagnetic material, such as iron, causes it became magnetized with no continuously.

As an external applied magnetizing field is changed, may be increased or decreased, the magnetization of the material changes discontinuously, causing “jump” in the magnetic flux through the ferromagnetic as shows in Fig. 2.11. In the very early finding, the jump was observed by using a coil of wire around the ferromagnetic bar, attached to an amplifier and speaker. The sudden transitions of the magnetization induce the current pulses in the coil, and makes a crackling sound. This sound, first discovered by German physicist Heinrich Barkhausen, and called *Barkhausen noise*.

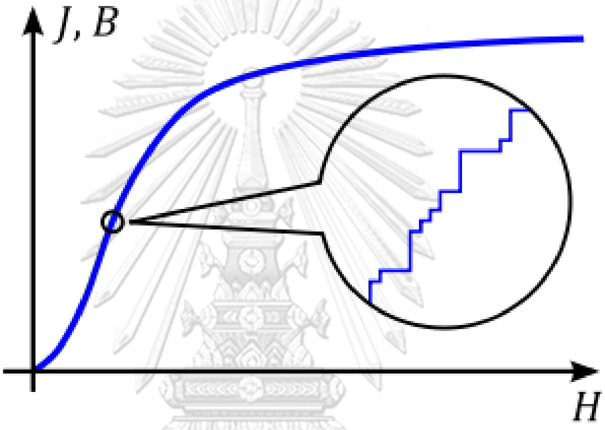

Fig. 2.11 Magnetization (J) or flux density (B) curve as function of magnetic field intensity (H) in ferromagnetic material (47).

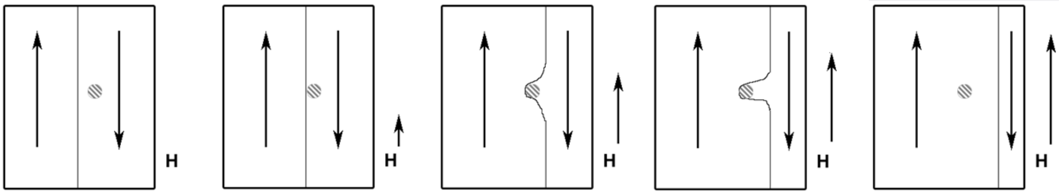

(a) (b) (c) (d) (e)

Fig. 2.12 Diagram of magnetization on ferromagnetic defected domains;(a) zero external field, (b) with external field and domain wall start moving, (c-d) at higher external field and domain wall distorted due to defect of material, and (e) at higher level external that can over the defect (47).

The magnetization jumps are from discrete changes of ferromagnetic domains. The magnetic domains are the clusters of atomic which have spins in the same direction for each domain. When apply the external magnetic field, the spins will be forced to align in the same direction according to the forcing field. At some point of external magnetizing field causing a sudden reversal of neighboring spins, and other whole domains suddenly turn into the direction of the external field, and creating the jump signal due to domain switching.

In some case, contamination or defect in ferromagnetic material could cause abnormal *Barkhausen jump*. In Fig. 2.12 (a) – (b), the domain wall started moving when the ferromagnetic has been applied the external field, and the domain wall is distorted due to contamination as shows in (c) and (d). Suddenly, the domain wall has been quickly changed from (d) to (e) and causing big jump.

2.3 Degradation of TMR magnetic thin film

Because of very thin and complexity of TMR magnetic film, the degradation of the layers would be very challenge issue. In the application of TMR, the bias voltage is applied to the thin film device. The breakdown on insulator layer is critical and interesting problem. The damaging could be *Intrinsic Breakdown* and *Extrinsic Breakdown*.

The obvious damaging could be due to combination of *electric field* and *heat* that effect to insulator layer which is the weakest layer of the device. If electric field is high enough, it would effect to ionize bonding of the dipole moment breakdown at some level of *activation energy*. The obvious damage could be explained by *E-Model* (48, 49) to explain the possibility of *Breakdown*, ***p(t)*** by equation (2.7).

$$p(t) = \mathrm{A}\exp(\frac{\mathrm{V(t)}}{\mathrm{B}}) \tag{2.7}$$

Where;

V(t) : Voltage across insulator thick $\mathbf{t_B}$ under electric field **E(t)** , and could be calculated from ;

$$\mathrm{V(t)} = \mathrm{E(t)} \times \mathrm{t}_B$$

A : Effect from thermal **(T)** and activation energy **($\mathbf{E_A}$)** in insulator area $\mathbf{A_J}$,

that calculated from ;

$$\mathrm{A} = \mathrm{A_J}\ \exp(\text{-}\mathrm{E_A}/\mathrm{kT})$$, **k** = Boltzmann's constant

B : Result of heat that effect to atoms of insulator thickness of $\mathbf{t_B}$

Case I : In case of atomic movement, calculated from;

$$\mathrm{B} = \mathrm{kTt_B}/\mathrm{a}\,|\mathrm{qZ}|$$

Where;

a = Atomic space

Z = Number of ion

q = Charge

At potential level that causes breakdown or called *"breakdown voltage"*, and relative to A and B.

$$V(t) \approx (\frac{B}{\mathrm{A}}) \tag{2.8}$$

Case II : In case of applied voltage increasing by time to the TMR thin film, the maximum voltage could be written as in (2.20).

$$V\max \approx B\ln\left(\frac{dV/dt}{\mathrm{AB}}\right) \tag{2.9}$$

From (2.7), we could see the breakdown point relates to *thickness* and *cross-section area* of the thin film. If consider within the same dimensions, we could observe the thinner film is easier broken down than the thicker film. Also the higher breakdown voltage is required for the higher temperature on thin film as shows in Fig. 2.13 – 2.14.

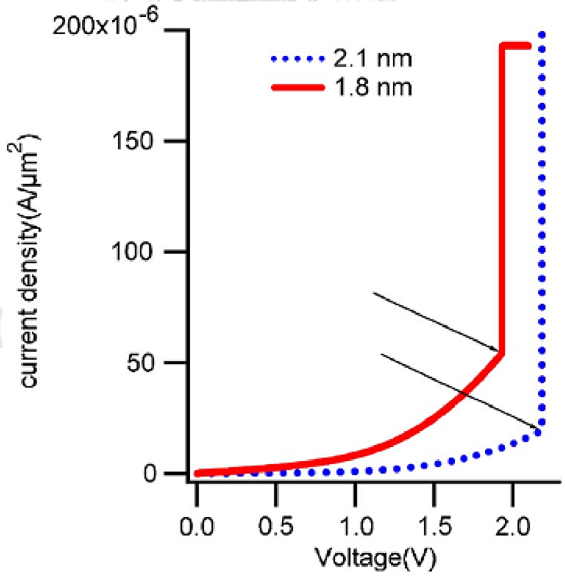

Fig. 2.13 Breakdown voltage of magnetic thin film comparison between 2.1 nm and 1.8 nm thickness (49).

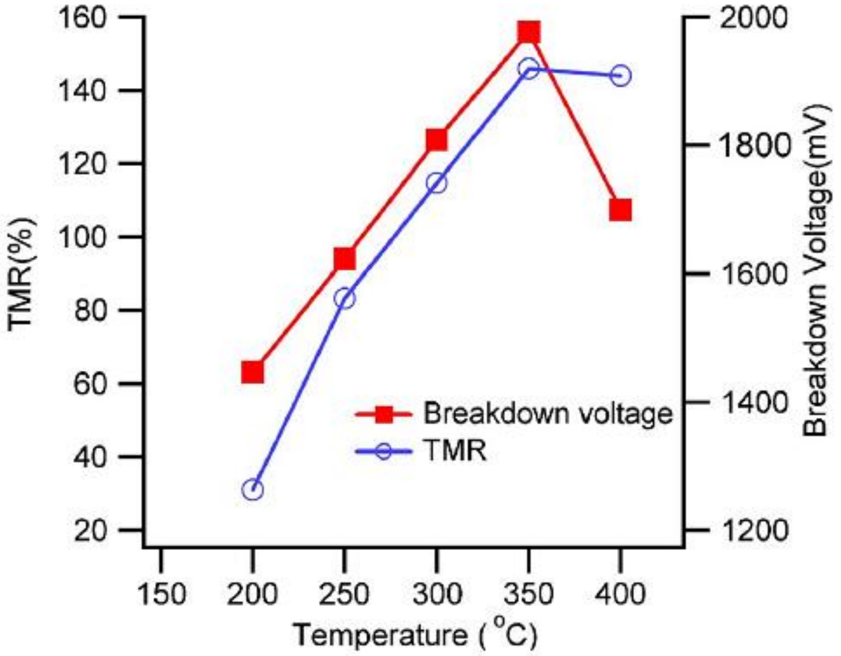

Fig. 2.14 Thermal effect on the breakdown voltage (49).

As the temperature increases, the breakdown voltage will be higher per equation (2.7). At the higher temperature we also observe higher TMR ratio. However, at about 350 ^{o}C, the breakdown voltage trend to be reduced when the TMR ration slightly decreases. The high temperature causes atomic lattice expansion, and ***B*** parameter is reduced, as a result of lower breakdown voltage. Up to about 350 ^{o}C, the MgO bonding may have more symmetry that why increasing of TMR ratio.

For the effect of *current bias direction*, *junction area*, and *parallel/antiparallel* condition were studied, and found they relate to the breakdown voltage and current density of TMR thin film. In Fig. 2.15, we could observe the bigger cross section area of TMR thin film has lower breakdown voltage, that could be explained in (2.7). For the same cross section area, the break down voltage relates to the electrodes polarity. The breakdown voltage of negative bias is lower than the breakdown voltage of positive bias. This finding is due to *spin filter effect* (49).

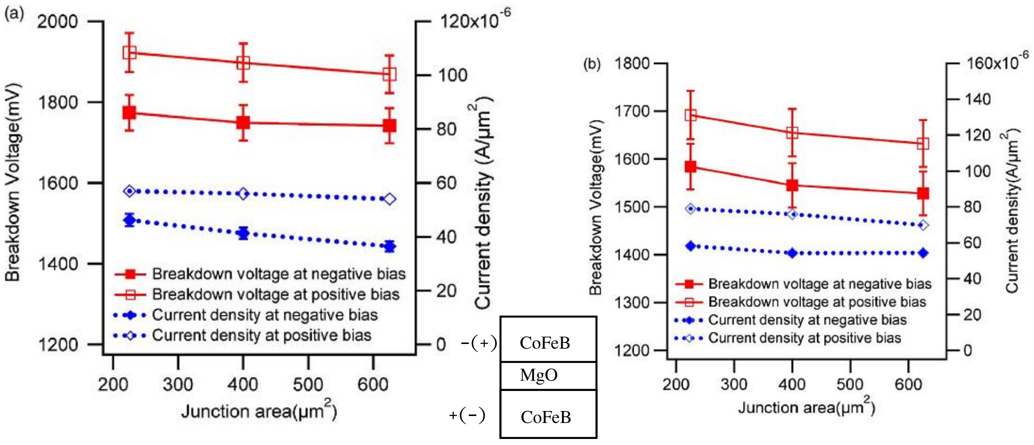

(a) (b)

Fig. 2.15 Cross sectional area of TMR thin film and breakdown voltage/current in forward and reverse bias ; (a) antiparallel TMR condition (b) parallel TMR condition (49).

The effect of *oxygen vacancy* of Fe/MgO/Fe has been studies by calculation, and found that oxygen vacancy effects to *transportation coefficient* (see Fig. 2.16) which would reduce the current flow and causes increasing in resistance, as a result of higher breakdown voltage (50).

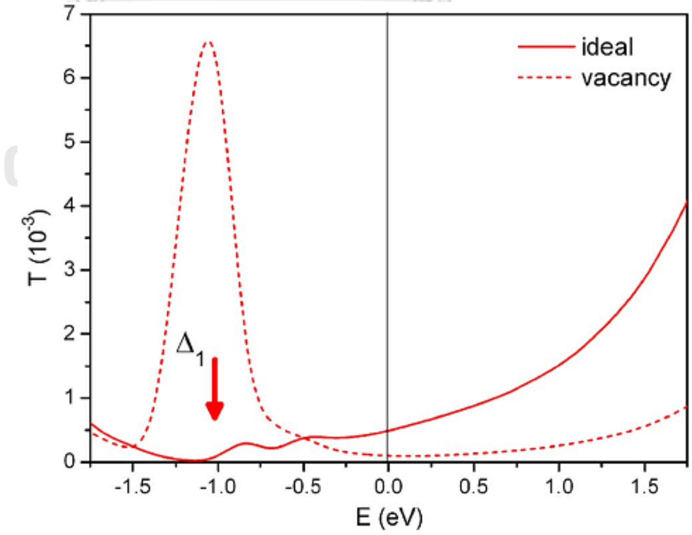

Fig. 2.16 Relative of energy (E) and transportation coefficient (T) of ideal magnetic thin film Fe/MgO/Fe (50).

In case of *pinhole* in the TMR, during apply the electric field, the pin hold might be expanded, and causing more leak current flow through the pin hole as a result of reducing in resistance ($R_{pinhole}$) as diagram shows in Fig. 2.17 (a). The pinholes could be represented by *parallel resistor circuit* in Fig. 2.17 (b).

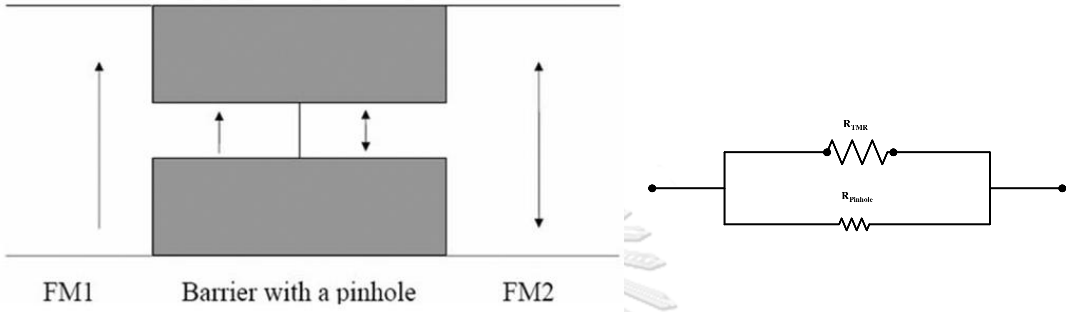

(a) (b)

Fig. 2.17 Diagram of TMR thin film with pin hole; (a) Pin hole in magnetic thin film TMR (51), (b) Circuit diagram of TMR resistance (R_{TMR}) and resistance of pin hole ($R_{pinhole}$).

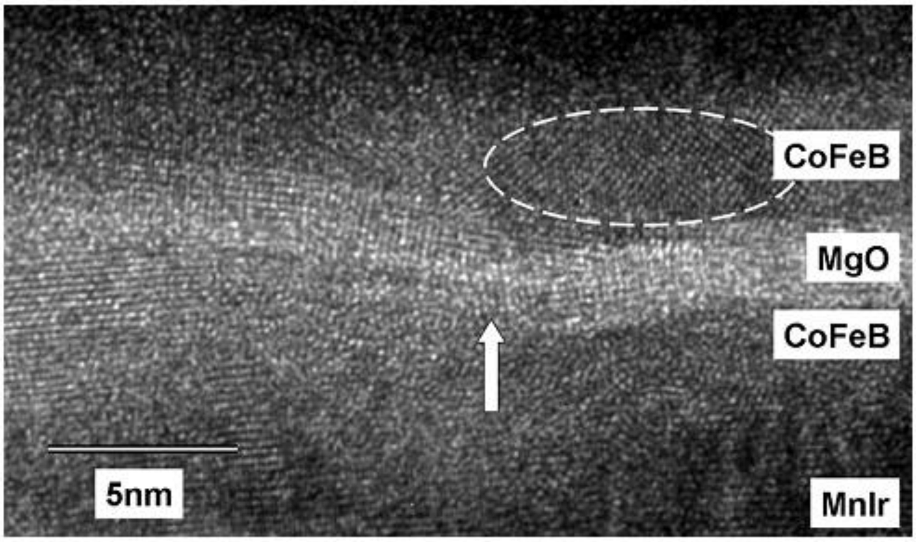

Fig. 2.18 TEM image of defect (pinhole) in magnetic thin film TMR (51).

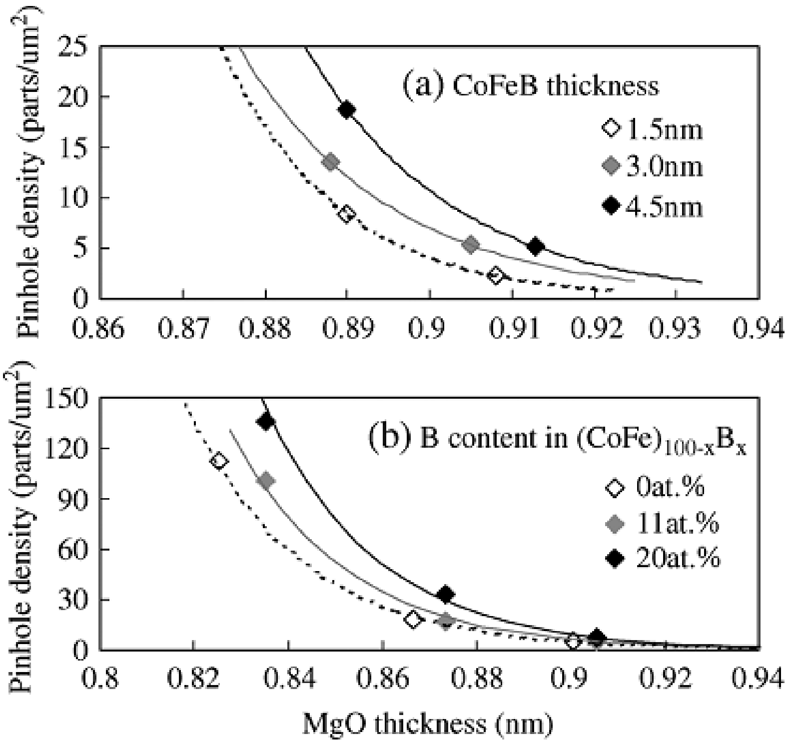

Fig. 2.19 Relation of MgO thickness and pinhole density; (a) Effect of CoFeB thickness to pinhole density, (b) Effect of B content to pinhole density (52).

MgO defect (pinhole) may be formed during thin film fabrication, and its density relates to the thickness of MgO layer (see Fig. 2.18). We could see the pinhole density reduce when the thickness of MgO increase In Fig. 2.19 (a), we have observed when the thickness of CoFeB layer increase, the pinhole density also increases. We also found the higher content of *boron* (B) in CoFeB/MgO/CoFeB components cause higher pinhole density as shows in Fig. 2.19 (b). This finding are possibly due to B diffusion in to MgO that causing more pinhole density (53, 54).

Out of voltage or current breakdown to the device, the thermal stress is important factor that cause the TMR degradation. It possibly came from thermal effects of *dynamic fly high* (DFH) element during operation, thermal effects from manufacturing process such as magnetic annealing, epoxy-curing process, electrostatic discharge and also thermal stress in reliability tests. In this work, we study the influence of thermal stress on TMR device degradation. The degradation of the device due to microstructural defects was analyzed to understand the possible cause that correlates to the degradation characteristic of individual device.

CHAPTER III

CHARACTERIZATIONS

In this chapter, the concept of characterization techniques that used in the study and analysis of TMR structures will be explained.

3.1 Quasi static tester

As we know, the TMR device has a resistance value that is corresponding to the applied magnetic field. The changes of resistance can also related to the relative angle between the magnetization direction of free layer and pinned layer. When the free layer magnetization direction is in parallel with the pinned layer, the electrons easily pass through the interface layers and give low resistance, but if the magnetization direction of free layer is in the opposite direction to the pinned later, the electrons difficulty pass the interface layers, and give high resistance. For magnetic recording data sensing function, the devices have been designed the free layer moving freely when the pinned later is fixed via magnetic coupling of antiferromagnetic layer.

The *quasi static tester* (QST) is used for testing the reader magnetically response of the devices. When the QST apply the electromagnetic field, the free layer magnetization will be rotated according to the applied field. The angle of free layer magnetization with respect to the pinned layer would relate to the magnitude of the QST applied field. This relative angle results in resistance-change due to TMR effect, and showed as “amplitude” in the QST measurement (with dc bias). With the higher applied electromagnetic field, the amplitude will be increased, and when the applied field goes opposite direction, the amplitude will give negative values. The plot between applied electromagnetic field (x-axis) and amplitude (y-axis) which shows relative of magnetic field and TMR response, called *“transfer curve”*, see Fig. 3.1 and

Fig. 3.2. The basic measurement parameters are; (1) MRR (static resistance of the reader under zero magnetic field), (2) amplitude (peak to peak voltage measured from the reader resistance change due to the apply magnetic field), (3) asymmetry (calculated symmetry of amplitude response for positive and negative magnetic field) and (4) barkhausen jump (7).

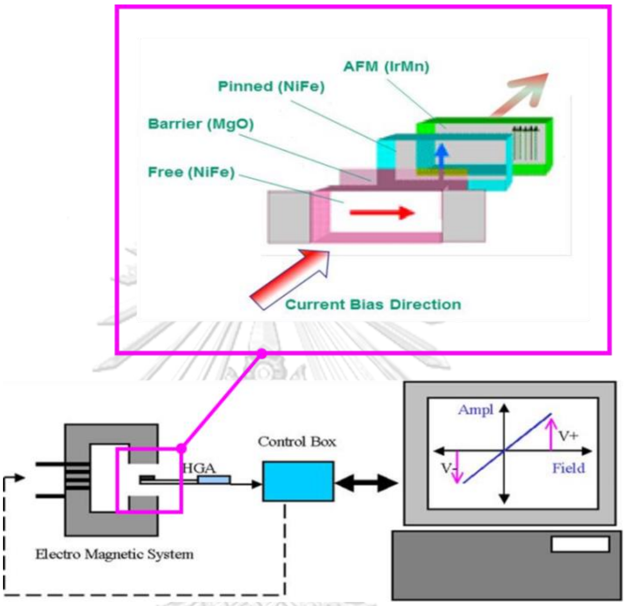

Fig. 3.1 Basic concept of Quasi Static Tester (QST) (7).

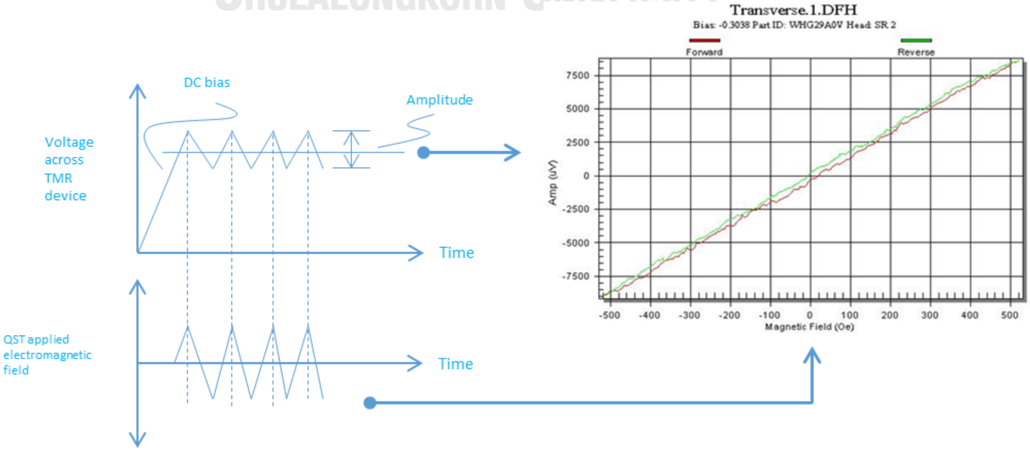

Fig. 3.2 QST bias and measurement (7).

In this dissertation work, the QST system model ISI 2012 from Integral Solutions has been used to measure the magnetic response of the TMR structure.

3.2 High-resolution transmission electron microscope (HTEM)

Over the limitation of Optical Microscope (OM), the Scanning Electron Microscope (SEM) has been use for the higher magnification with the break through technique, form optical to electron incident. For the higher magnification that is the limit of SEM, the Transmission Electron Microscopy (TEM) is a powerful equipment using for nano-scale inspection of materials (55).

The first TEM was developed by Max Knoll and Ernst Ruska in 1931, and the first commercial TEM was in 1939. Ruska was awarded the Nobel Prize in physics for the development of transmission electron microscopy in 1986.

TEM technique uses a beam of electrons transition through a specimen to form an image. So, the specimen is needed to be prepared very thin less than 100 nm thick. The electron beam is transmitted through the specimen to form the image onto imaging unit such as screen, film or a sensor such as a charge-coupled device (CCD). The information could be applied for understanding the microstructure and composition of the. The contrast of the image is developed from the transmitted electrons through the specimen with the scattering mechanisms which is interaction between electrons and atomic of the sample. There are two mode that generally be used; (1) imaging mode and (2) diffraction mode. A schematic picture of TEM is showed on Fig. 3.3.

High-Resolution Electron Microscope (HRTEM) that could give the quality image uses a large diameter object aperture that help induce several diffraction beam, and the beam passed through the objective aperture then form the image. In high magnification, and high resolution, we could obtain contrast in the image with periodic fringes (phase contrast). These fringes represent a direct resolution of the

Gragg's diffraction planes, and the fringes that are observed in high resolution images are from Bragge's reflecting planes.

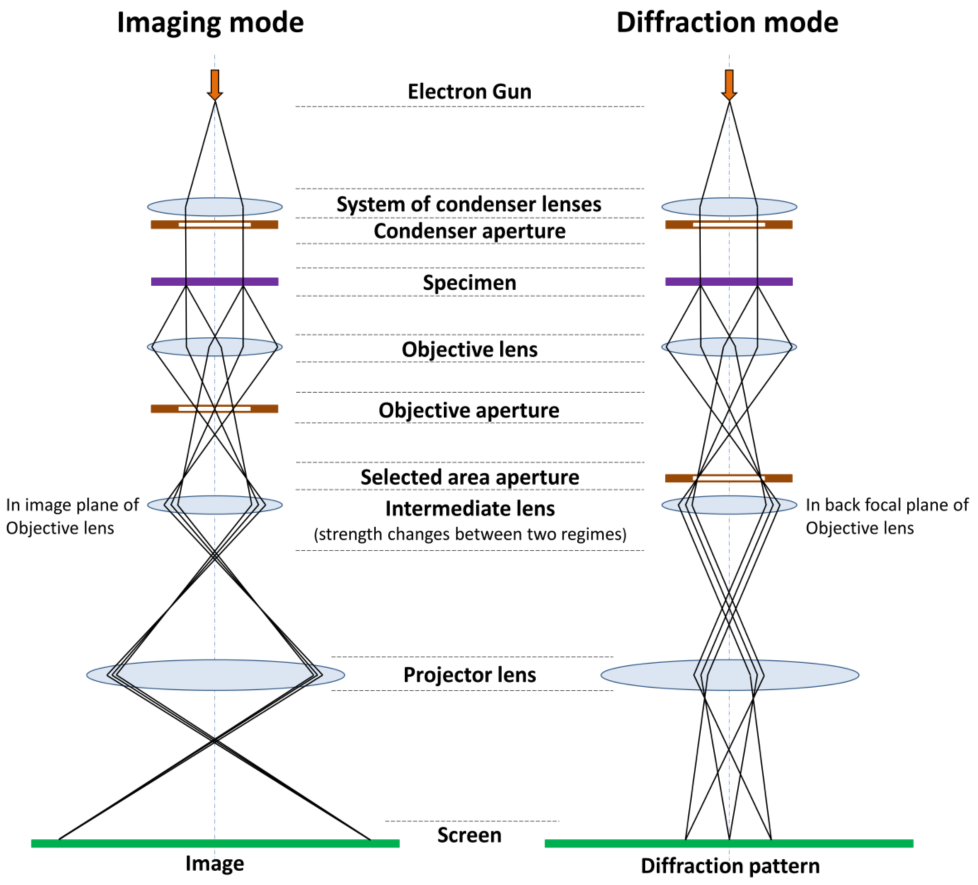

Fig. 3.3 Schematic of Transmission Electron Microscope (TEM); (a) Imaging mode and (b) Diffraction mode (55).

In this research, an FEI Titan3 G2 TEM and FEI-Osiris scanning transmission electron microscopy (STEM) were used to investigate the microstructure of the TMR device. The TEM samples were prepared by using FIB techniques, and the details of FIB will be described in the next section.

3.3 Focus ion beam (FIB)

Focused ion beam (FIB) is a technique used for analysis, deposition, and ablation of materials. It is a scientific instrument that normally resembles in a scanning electron microscope (SEM). The FIB has been used in the high technology analysis lab such as application for defect analysis on transmission electron microscope (TEM) sample preparation. The instrument is using *liquid metal ion sources* (LMIS), such as gallium ion (Ga), gold (Au) and iridium (Ir) (56).

In a gallium LMIS, gallium metal is put in contact with a tungsten needle. We heat the liquid gallium and flows to the tip of the needle. The tip radius is extremely small (~2 nm), and the very high electric field has been applied to this small tip (greater than 1 x 10^8 volts per centimeter) to induce ionization and field emission of the gallium atoms. The ions are accelerated to 1–50 keV (kiloelectronvolts), and focused onto the sample by electrostatic lenses for the etching process. The very fine etching help to achieve very thin and smooth surface of the sample preparation for HRTEM to have high quality images. The schematic of FIB instrument shows in Fig.3.4, and the sample preparation shows in Fig 3.5, respectively. The focused ion beam used in this work is FEI Helios 450s.

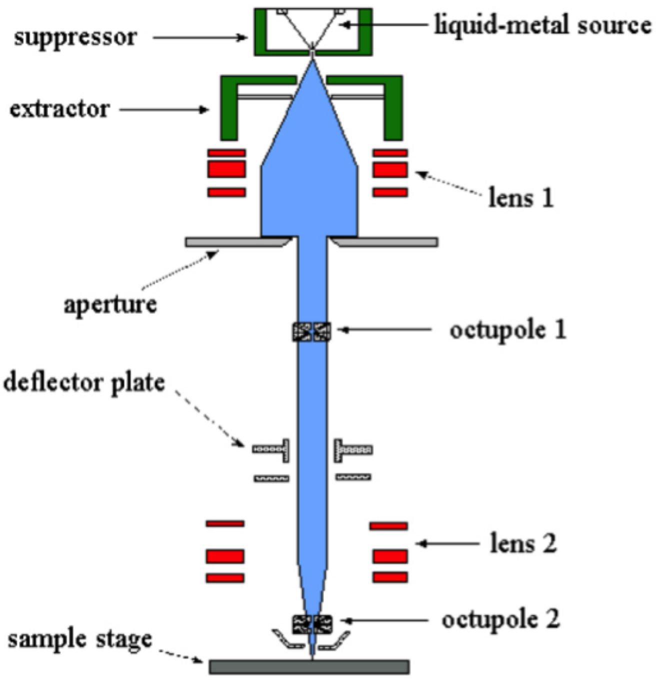

Fig. 3.4 Schematic of Focus Ion Beam (FIB) instrument (56).

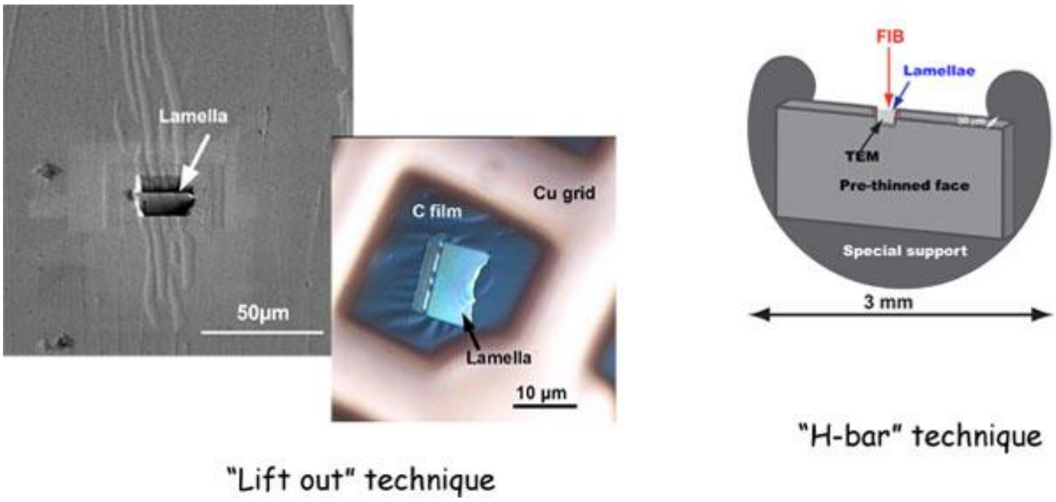

"Lift out" technique

"H-bar" technique

Fig. 3.5 Focus Ion Beam (FIB) sample preparation by using FIB (56).

3.4 Energy dispersive X-ray (EDX)

Energy Dispersive X-ray instrument is used for analysis and characterize the materials. The technique is using high energy electron beam to stimulate the specimen for emitting the X-ray. Each material has individual X-ray spectrum due to individual characteristic of K, L and M energy levels, so we could know the material types of the sample via analysis of the signal from the detector (see Fig. 3.6 - 3.7) (57).

The signal intensity of the signals would relate to the composition of elements, so we also know the percentage combination of the alloy elements by using this technique. The detected energies are also being mapped with the TEM image which help enhance the material distribution analysis as shows example in Fig 3.8.

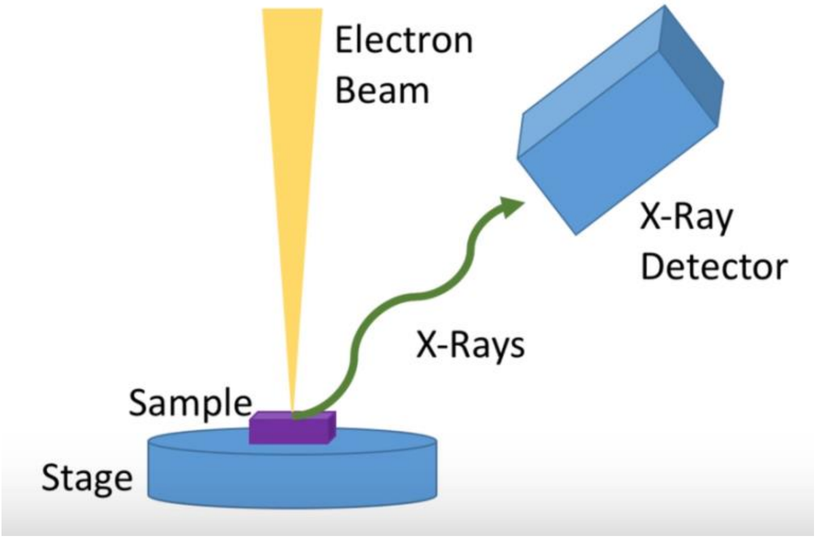

Fig. 3.6 Schematic of Energy Dispersive X-ray (EDX) equipment (57).

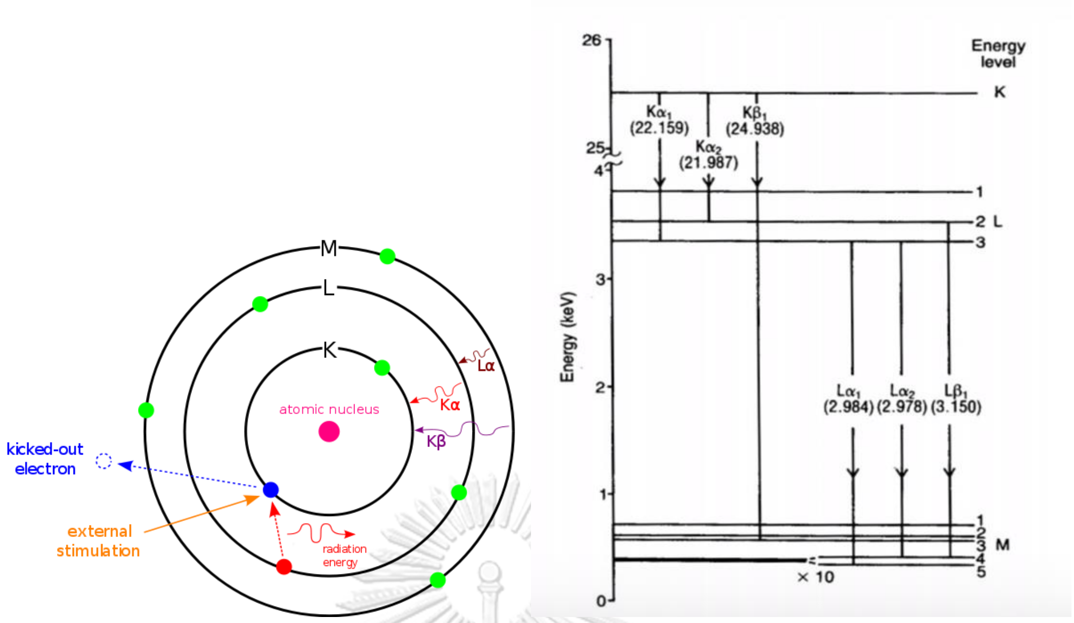

Fig 3.7 X-ray characteristic of material (57)

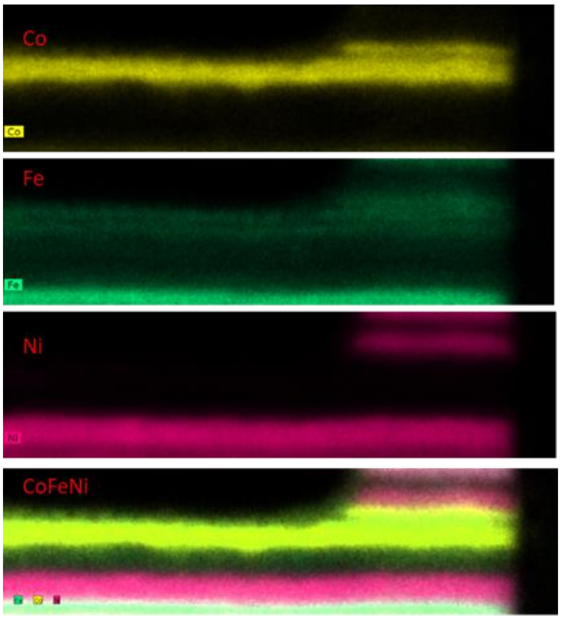

Fig. 3.8 Example of X-ray energy mapping analysis

In this research, an FEI Titan3 G2 TEM and FEI-Osiris scanning transmission electron microscopy (STEM), equipped with a BRUKER Super-XEDX Esprit, were used to investigate the microstructure and elemental mapping of the layers with the electron microscopes operating at 200 kV. The elemental mapping from the energy-dispersive X-ray spectroscopy (XEDS) were performed for all the key elements within the TMR structure.

In SEM an electron beam is focused into a small probe across the surface of a specimen. Several interactions with the sample that result in the emission of electrons or photons occur as the electrons penetrate the surface. These emitted particles can be collected with the detector to give information about the material. The resolution is determined by beam diameter. When in transmission electron microscopy (TEM), a beam of highly focused electrons are directed toward a thinned sample (<200 nm). It is very high resolution, compared to SEM. These highly energetic incident electrons interact with the atoms in the sample producing characteristic radiation and particles providing information for materials characterization. Information is obtained from both deflected and non-deflected transmitted electrons, backscattered and secondary electrons, and emitted photons. The resolution of a scanning electron microscope is lower than that of a transmission electron microscope. While TEM can view the images of objects to atomic level (which is less than 1nm), SEM can only be used to view images that require tens of nm at most.

CHAPTER IV

EXPERIMENTAL

The experiment has been separated into three parts, each part would give different view point, and to have combination results would help better understanding of heat effect on TMR device degradation.

Part 1. Thermal stress study by using heater module annealing; this method is good to represent general heat source effect such as thermal from IR oven in HGA process, from magnetic annealing in Slider fabrication process, but weak point of this method we do not know nano-structure of TMR device before stress.

Part 2. Thermal stress study by using in-situ annealing equip with TEM; this method is good to observed the changing of nano-structure during thermally stress, but weak point we cannot measure QST of the TMR device after stress.

Part 3. Thermal stress study by using laser excitation; this method is good to represent irradiation induce heat on TMR device which may represent laser beam reflecting in HAMR, PSA/RSA adjust by laser, Laser attached process. Weak point of this method, we also do not know the TMR structure before stress, also difficult to measure the accurate temperature on the device.

4.1 TMR device structure for experiment

The TMR devices used in the experiments were the embedded in HDD magnetic heads which were fabricated by physical vapor deposition (PVD) processes on Al2O3-TiC (AlTiC) substrates. The main structure of the TMR device composes of a magnetically free layer, a tunneling barrier, a pinned layer, and pinning layer. The free layer and pinned layer are made of soft magnetic materials such as NiFe, NiFeB, CoFe or CoFeB and the pinning layer is made of antiferromagnetic materials such as IrMn. The barrier layer is usually made from very thin insulator material such as MgO or Al2O3, to create magnetic tunneling effect. In this work, MgO has been used since it gives better performance than Al2O3, due to its crystal structure (12). The crystallinity helps to minimize electrons scattering over those amorphous structures (13). To improve the magnetic exchange-biasing between the pinned layer and the pinning layer, another soft magnetic layer has been added, isolated by a layer of nonmagnetic material such as Ta and Ru as a buffer layer. This enhanced design is called synthetic ferromagnetic structure (14-16). The schematic diagram of this device structure is illustrated in Fig. 4.1. The wafers were passed through a slider fabrication process, which composed of many process such as dicing, lapping, cutting, ABS formation and head overcoat deposition. The finished devices were measured for the electrical characteristics and investigated for microstructural defects due to applied thermal stress.

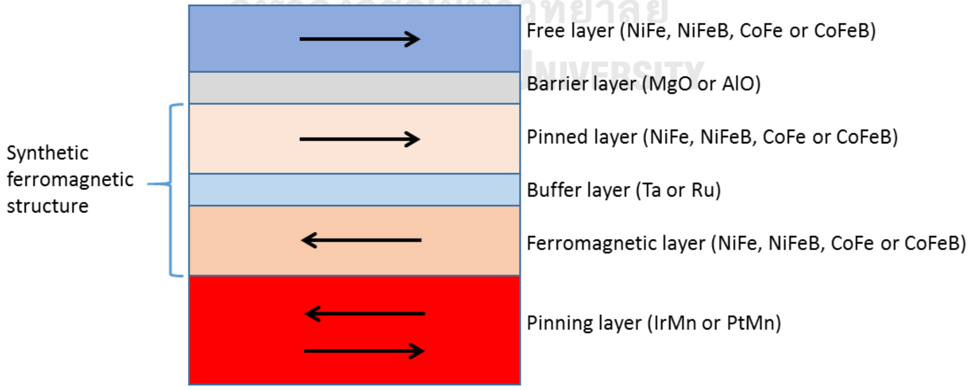

Fig. 4.1 Schematic diagram of synthetic ferromagnetic structure of TMR device

4.2 Experiment setup and characterization method

4.2.1 Thermal stress study by using heater module annealing procedure

The quasi static test (QST) method was used to investigate the TMR device characteristics. QST consists of an electromagnetic core, a control box, and computer control unit. The TMR device is placed in the gap of electro-magnetic core, and the DC bias is then applied to the TMR device to measure the resistance change as a function of the external electromagnetic field to simulate the field of magnetic data (17).

For thermal stress measurement, the TMR devices were grouped (ten devices for each group), and measured resistance, amplitude and asymmetry parameters by a commercially available QST tester from integral solution international (ISI). The measurement setup was 140 mV bias with the magnetic field sweep +/- 519 Oe, and magnetic field step 1 Oe. Then the devices were thermally stressed in a furnace between 150-250°Cfor 30 minutes, while the control group was kept at room temperature. The flow of experiment is showed in Fig.4.2.

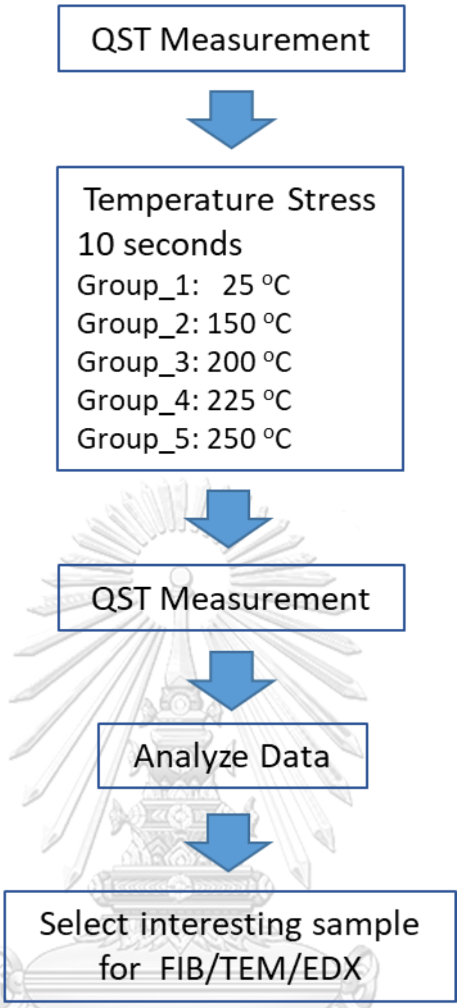

Fig. 4.2 Thermal stress experiment flow.

The thermal module used in the experiment composes of temperature controller, a heater unit, and a thermocouple with temperature feedback control as shows in Fig. 4.3.

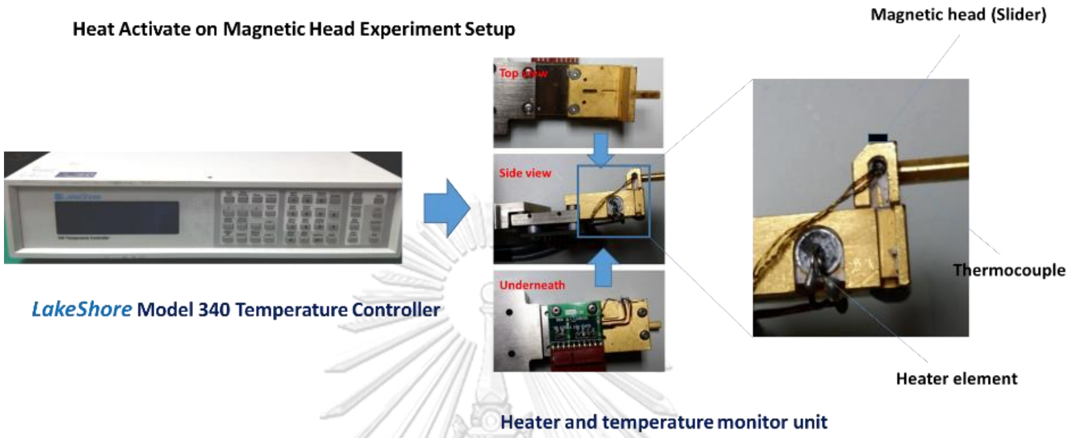

Fig. 4.3 Thermal stress experiment module and setup.

After the thermal stress, the TMR devices were re-measured for the QST parameters again, and the changes in percentage were calculated for resistance, amplitude and asymmetry parameters. The cross-sectional microstructure and elemental analysis were investigated using TEM, STEM, and XEDS to study the structure defects which corresponding to the QST parametric changes. The TEM samples preparation was done using FIB (FEI Helios 450s). TEM (Titan 3TM G2 60-300) and STEM (FEI Osiris) equipped with XEDS (BRUKER) were used to investigate the microstructure and interfaces between the layers.

4.2.2 Thermal stress study by using in-situ annealing equip with TEM

This experiment, the sample has been prepared by using FIB (FEI Helios 450s), and loaded on the heat source fixture which was built-in the TEM (Titan 3TM G2 60-300). This TEM is capable to taken the image in real time during thermally stress on the device which is very powerful tool to observe the material structure with very high resolution in the level of nanometer scale. The thermal stress was started temperature from 25 ^{o}C, then increased to 150 ^{o}C, 250 ^{o}C and 350 ^{o}C., each step the thermal stress was 30 minutes applied.

4.2.3 Thermal stress study by using laser excitation

In this experiment, the TMR reader sensors were measured the magnetic response properties by using the quasi static tester (QST), then beam the 1,000 mW laser onto the reader sensor area for 10 seconds. After that, the reader sensors were re-measured magnetic response by QST again. These sequential steps were repeated for 20 cycles of each heads. The experiment was performed on tree samples when another two heads were measured only QST without stressing which was used for reference heads. The flow of experiment is showed in Fig. 4.4, and the laser beam stress setup is showed in Fig. 4.5.

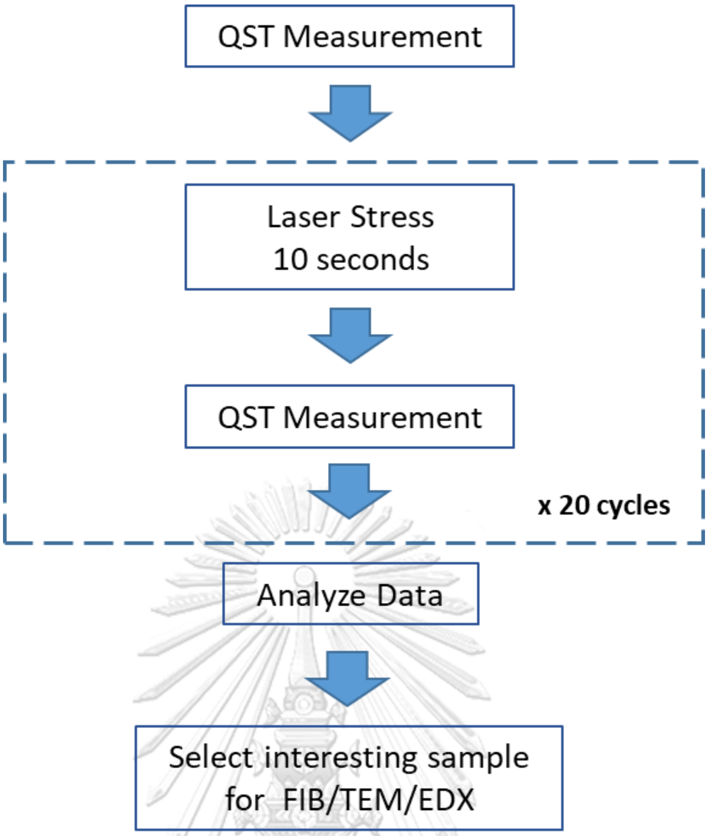

Fig. 4.4 Laser stress experiment flow.

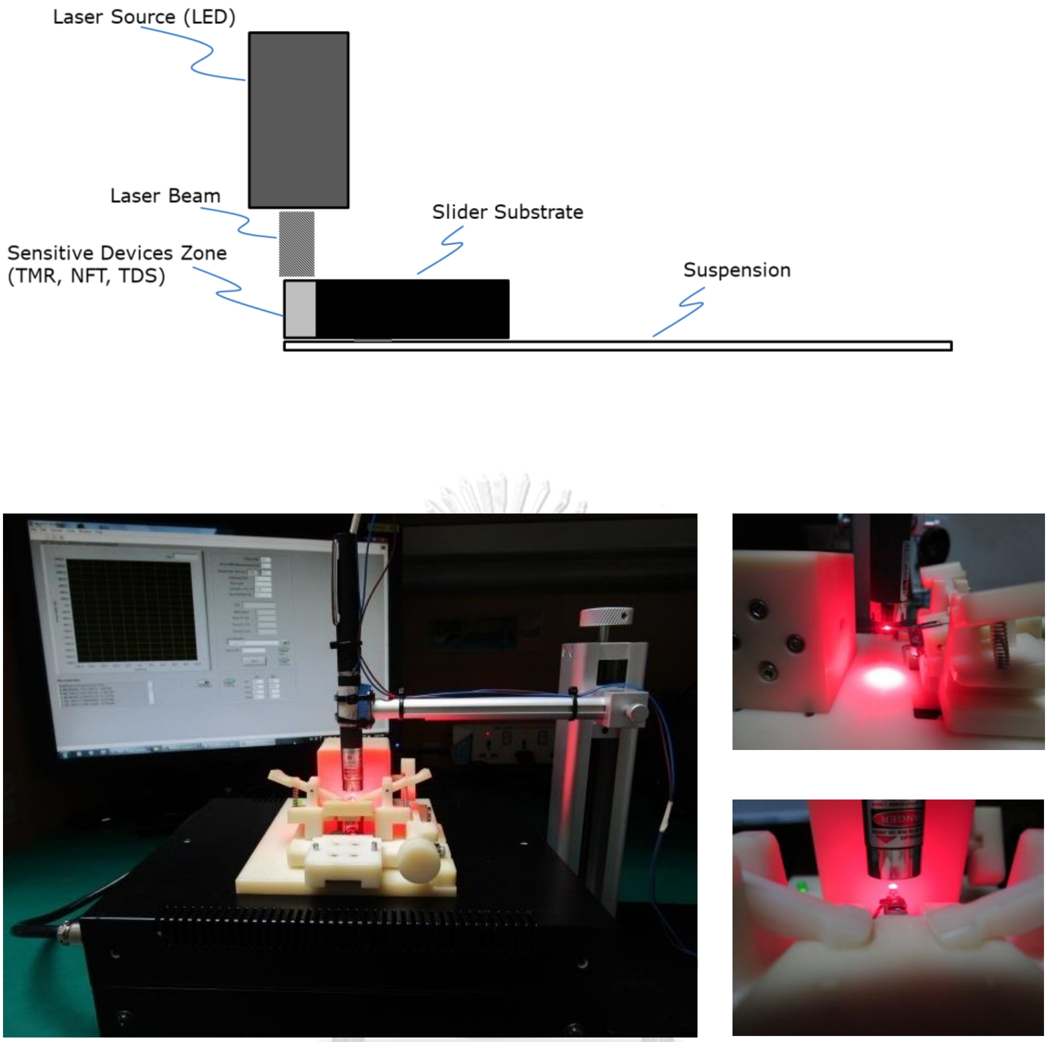

Fig. 4.5 Laser stress on magnetic head experiment setup

CHAPTER V

RESULTS AND DISCUSSION

5.1 Thermal stress study by using heater module annealing

Normally, the resistance of the TMR device can be changed when the magnetic field has been applied in direction perpendicular to the device. The change in resistance is due to spin-dependent transportation across the spacer layer. It relates to the relative angle between the magnetization direction of free layer and pinned layer. As the free layer magnetization direction aligns in parallel with the direction of the pinned layer, the electrons can easily transport through the interface between those 2 layers and exhibit a low resistance. On the other hand, if the magnetization direction of free layer is in the opposite direction to the pinned layer, electrons transport through the interface is difficult, and a high resistance results. This device has been designed that the magnetization direction of free layer can be moved freely when the pinned layer is fixed via magnetic coupling of antiferromagnetic layer [1-2].

Results from QST measurements before and after applied thermal stress are shown in Fig. 5.1 (a) - (c) and be summarized in Table 1. The result from Fig.5.1 (a) shows that at higher temperature, the percentage change in resistance at zero field (%ΔMRR) values start to increase, as seen by an increase of the mean value and STD of the %ΔMRR in Table 1. For the percentage change in QST amplitude after thermal stress with the stress temperature (%ΔAmplitude), It was found that some devices have more increasing percentage at higher temperature when some devices have more reducing percentage than others, as shows in Fig 5.1 (b). In Table 1, the STD of the %ΔAmplitude starts to increase at higher temperatures, when the mean value of percentage change in amplitude is almost constant because we observed both increased and decreased amplitude. Fig. 5.1 (c) shows percentage change in QST asymmetry (%ΔAsymmetry) after thermal stress.

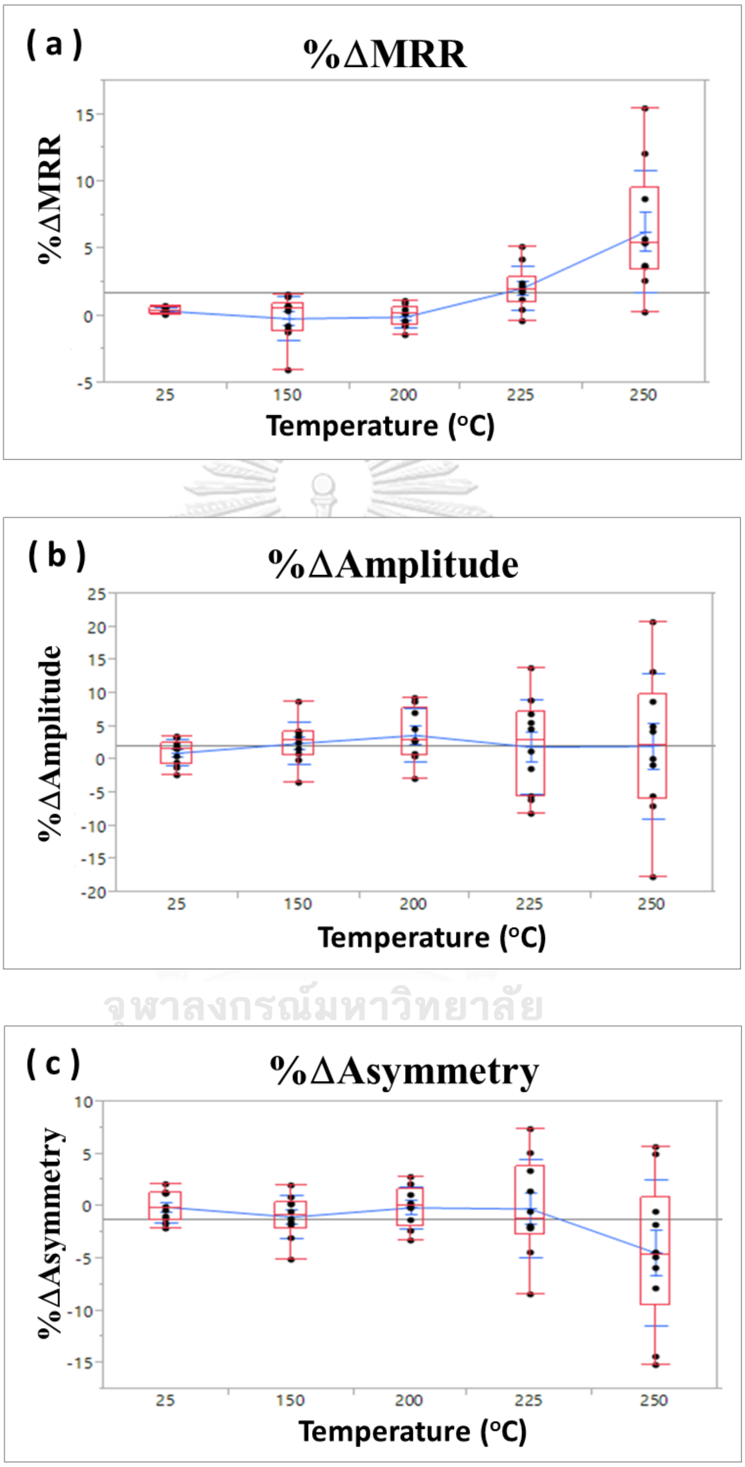

Fig. 5.1 Percentage change of QST parameters versus stress temperature ; (a) %ΔMRR versus stress temperature, (b) %ΔAmplitude versus stress temperature, and (c) %ΔAsymmetry versus stress temperature.

Table 5.1 Statistical values of the measured QST parameters versus stress temperature.

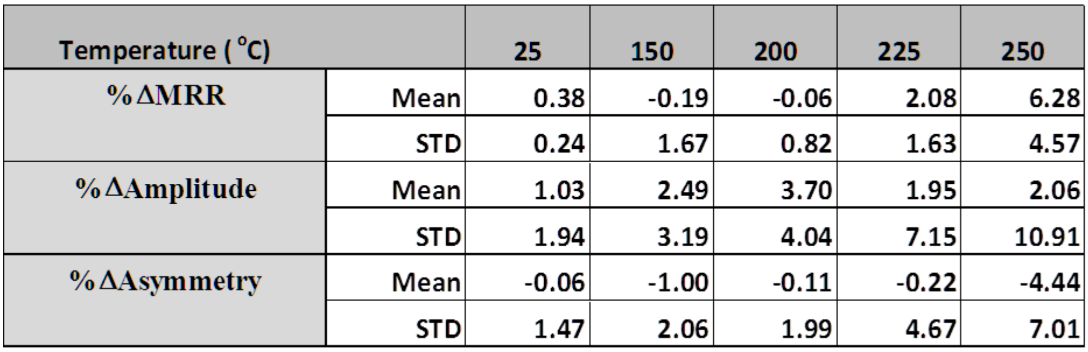

Temperature (°C)		25	150	200	225	250
%ΔMRR	Mean	0.38	-0.19	-0.06	2.08	6.28
	STD	0.24	1.67	0.82	1.63	4.57
%ΔAmplitude	Mean	1.03	2.49	3.70	1.95	2.06
	STD	1.94	3.19	4.04	7.15	10.91
%ΔAsymmetry	Mean	-0.06	-1.00	-0.11	-0.22	-4.44
	STD	1.47	2.06	1.99	4.67	7.01

It was found that at the higher temperature, the %ΔAsymmetry decreased, obviously at 225℃. In addition, at stress temperature about 250℃, a device was observed a noisy curve from the QST measurement and the appearance of a spike peak known as Barkhausen jump, which is clearly seen on the forward QST test at 180 Oe as shows in Fig 5.2. This Barkhausen jump normally can be caused by multi-domain of ferromagnetic layers such as free layer or pinned layers has suddenly switched during QST measurement [51].

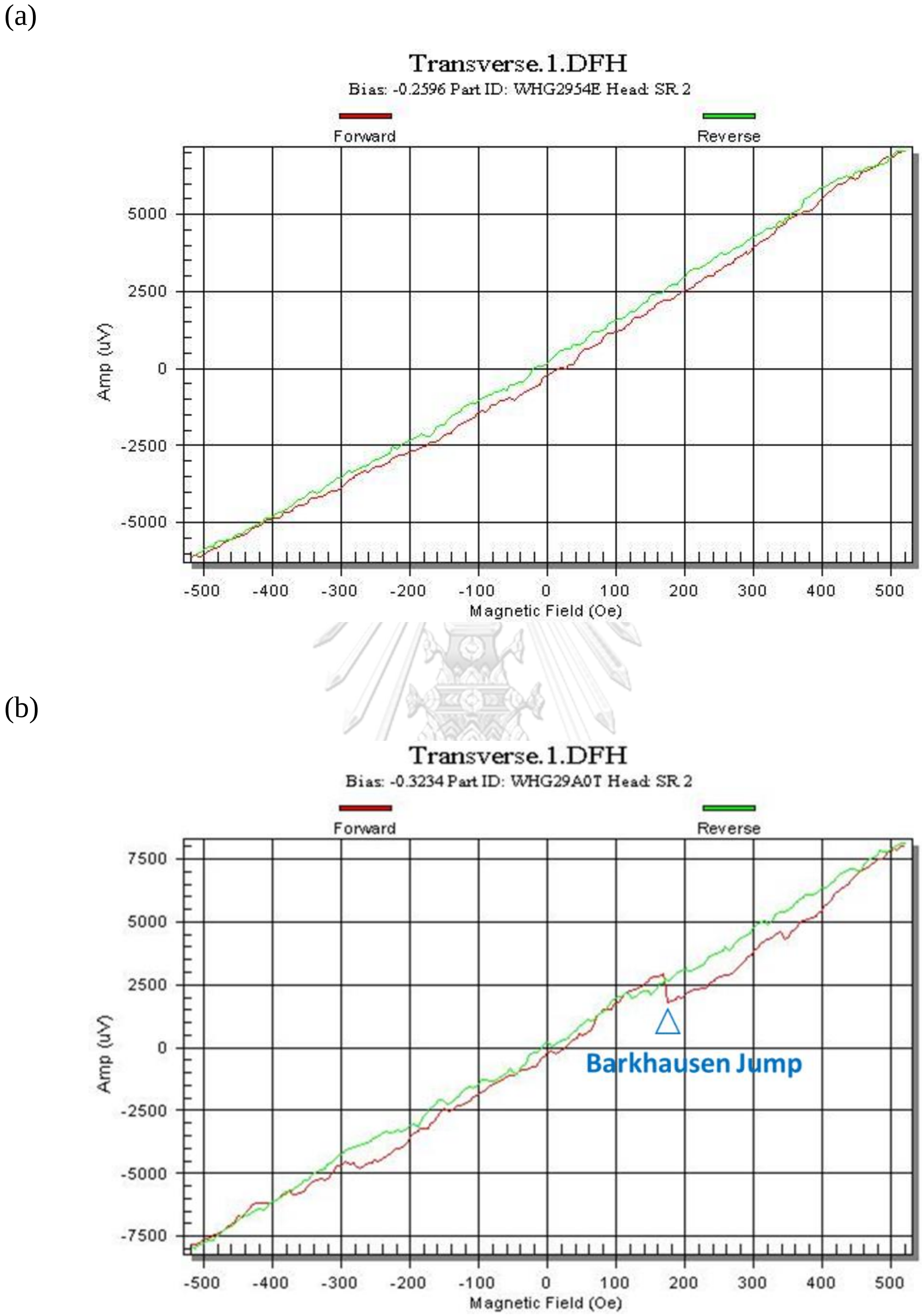

Fig. 5.2 QST Transfer curve ; (a) Transfer curve of normal device and (b) Transfer curve of thermally stressed device at 250 ^{o}C that was observed Barkhausen jump at 180 Oe.

For microstructural analysis, the cross-sectional transmission electron and scanning transmission electron micrographs of the thermal stressed device at 250°C are in Fig. 5.3 (a) and (b). The micrographs clearly show the interfaces between layers in the multilayer TMR device structure. As shown in Fig. 5.4 (a) and (b), at the MgO barrier, we observe the recrystallization and discontinuity of the MgO atomic planes in some part of the layer, which is not found in the reference device without thermal stress. Normally, the MgO barrier layer requires good crystallinity to maximize electron transport and minimize electron scattering. The result from EDX analysis of MgO layer also shows inhomogeneity of Mg in MgO layer. This layer defect could cause electrons scattering that induce high resistance and noisy signal. It can also be possible that the high percentage change in resistance and the noisy transfer curve could be affected from the degradation of barrier layer caused by inhomogeneity of Mg due to thermal stress.

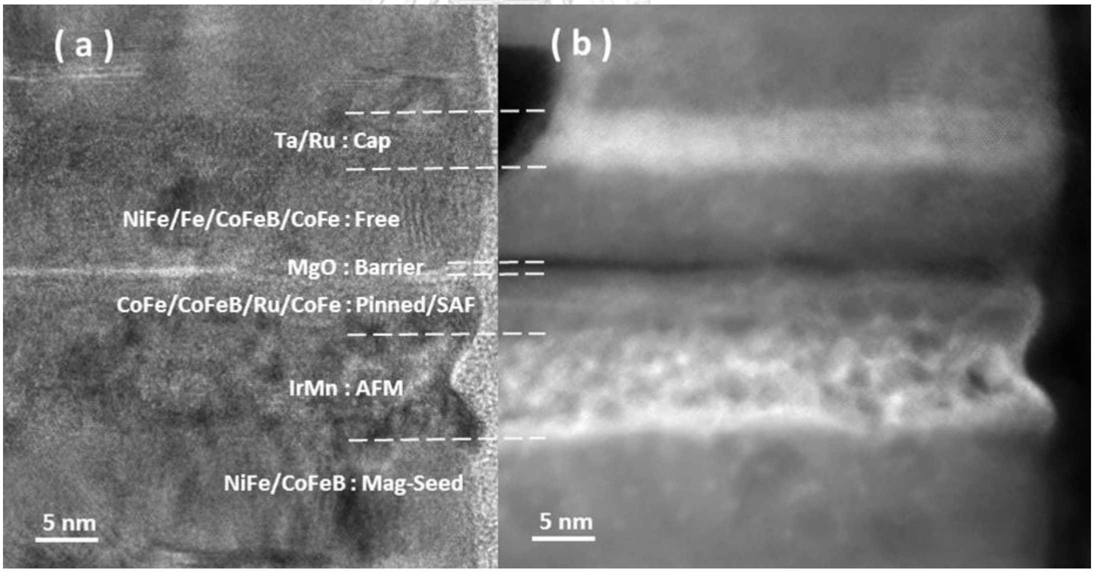

Fig. 5.3 Cross-sectional electron micrographs of TMR device after induce thermal stress at 250°C in (a) TEM mode and (b) STEM mode.

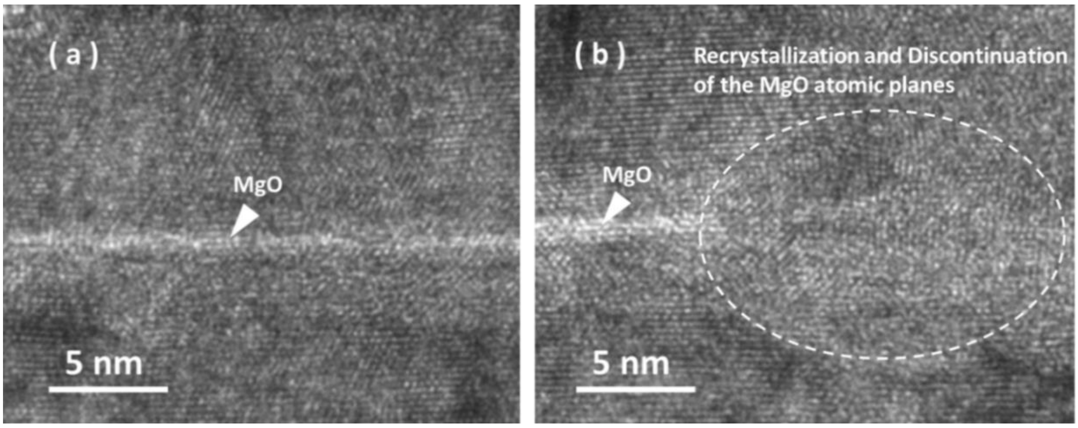

Fig. 5.4 Cross-sectional electron micrographs at barrier layer of TMR device (a) normal and (b) after applying thermal stress at 250℃.

The EDX analysis on AFM layer also indicated the Mn depletion within IrMn layer as shown in Fig. 5.5. The function of IrMn AFM layer in TMR device is to pin the pinned layer. The depletion of Mn could lead to a poor magnetic exchange-coupling force to the pinned layer and cause magnetic multi-domain in the reference layer. If a portion of the multi-domain has suddenly switched, the QST transfer curve could exhibit Barkhausen jump. Thus, the Mn depletion may be a part of Barkhausen jump at 180 Oe forward QST test. Others layers are also analyzed, but no abnormal defect was observed as show in Fig. 5.6.

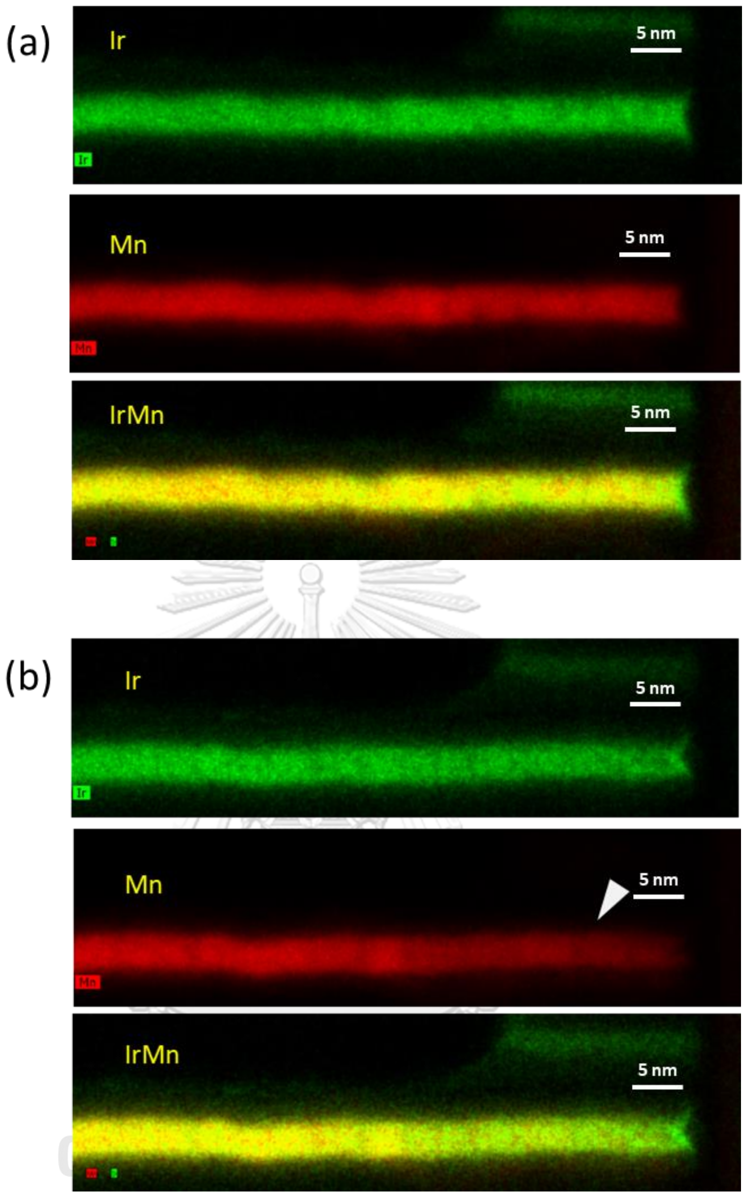

Fig. 5.5 (a) XEDS analysis of normal AFM of TMR device, and (b) the Mn depletion of the IrMn AFM layer of the thermal stress TMR device.

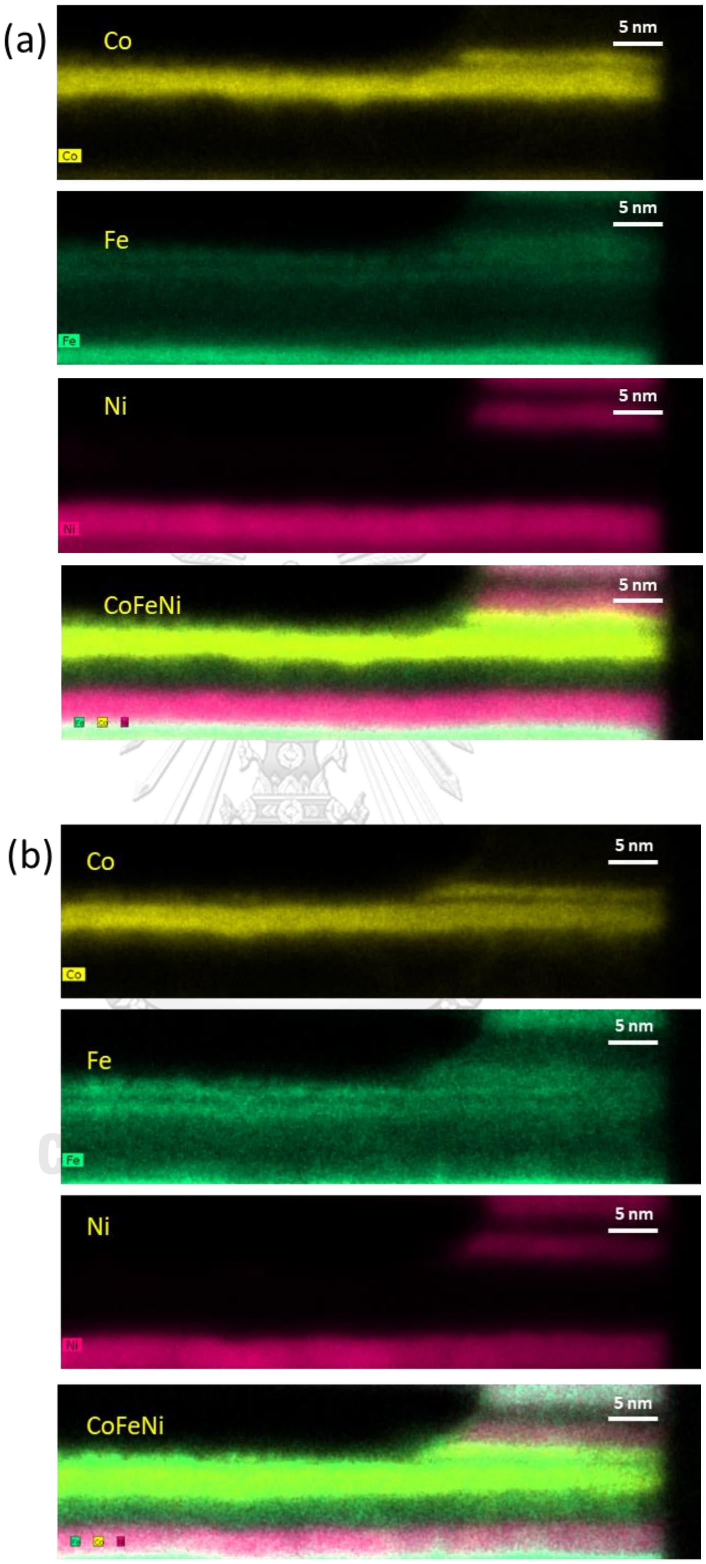

Fig. 5.6 (b) XEDS analysis of Co/Fe/Ni composition for normal TMR device and (b) for the thermal stress TMR device.

From the microstructural analysis observation, we believed that one of the major reasons of increasing the %ΔMRR could be due to the barrier layer change such as re-crystallization and atomic interfacing with the adjacent ferromagnetic layers of both pinned and free layers after the thermal stress. This can cause an obstruction of electron transportation as a result of higher resistance behavior.

In some cases of the increasing of %ΔAmplitude can be due to an improvement of crystal structure of some devices materials caused by the annealing process induces structural relaxation and help to increase the amplitude values. However, for some devices the thermal stress from annealing can create some structure defects and cause the reduction of the amplitude value.

The %ΔAsymmetry decreased can be caused by the changing of bias point of the devices, possibly due to the modification of synthetic pinning structure such as re-crystallization, interface effects between layers or materials inter-diffusion affecting to magnetic coupling to the pinning behavior.

5.2 Thermal stress study by using in-situ annealing equip with TEM

To be able to observe the changing in the microstructure of the materials in different layers of TMR structure, the slider was prepared by FIB before investigated in the transmission electron microscope. A special TEM holder with a heater was used to anneal the sample inside the microscope and simultaneously investigated by high angle annular dark field scanning transmission electron microscopy (HAADF-STEM) and electron energy loss spectroscopy (STEM-EELS) in the Linköping FEI Titan3 60-300, equipped with a Gatan Quantum ERS. The electron microscope was operated at the working acceleration voltage of 300 kV.

The *in-situ* real-time annealing TEM study showed the images of sample stressed temperature lower than 250 °C were hardly observed the change in microstructure of the TMR, when the 350 °C image was observed part of ultra-thin Ru layer interfaces that was not an abrupt as original at 25 °C. This is a sign indicate a diffusion of materials via the interfaces. The observation of changing in Ru layer could imply that materials compose of TMR which have atomic weight less than Ru (101.07) such as B (10.81), Fe (55.85), Ni (58.70), Co (58.93), Mg (24.31), O (15.99) and Mn (54.94), could diffuse to adjacent layers and causing instability. The AFM layer was also observed structure change at this stress temperature, see Fig. 5.7.

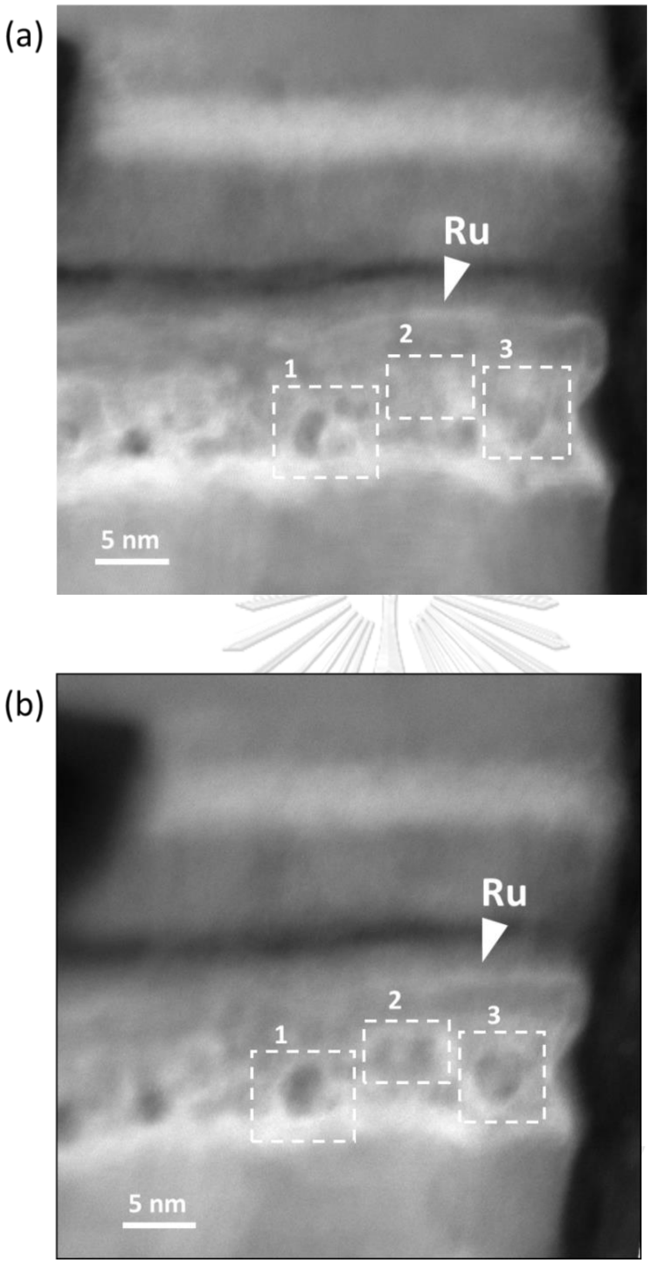

Fig. 5.7. (a) TEM image (STEM mode) of TMR on *in-situ* annealing equipment at 25 ^{o}C, and (b) after thermal stress to 350 ^{o}C, observed diffusion of Ru into adjacent soft magnetic layers and the crystal structure changes of IrMn AFM layer

5.3 Thermal stress study by using laser excitation

After the TMR devices were thermally stressed by the laser beam, percentage change of QST has investigated as the results shown in Fig 5.8. The MRR and asymmetry parameters were not observed significantly change, when the amplitude parameter was observed decreasing on HD#1 (-7.45%), HD#2 (-24.56%) and HD#3 (-63.43%), respectively.

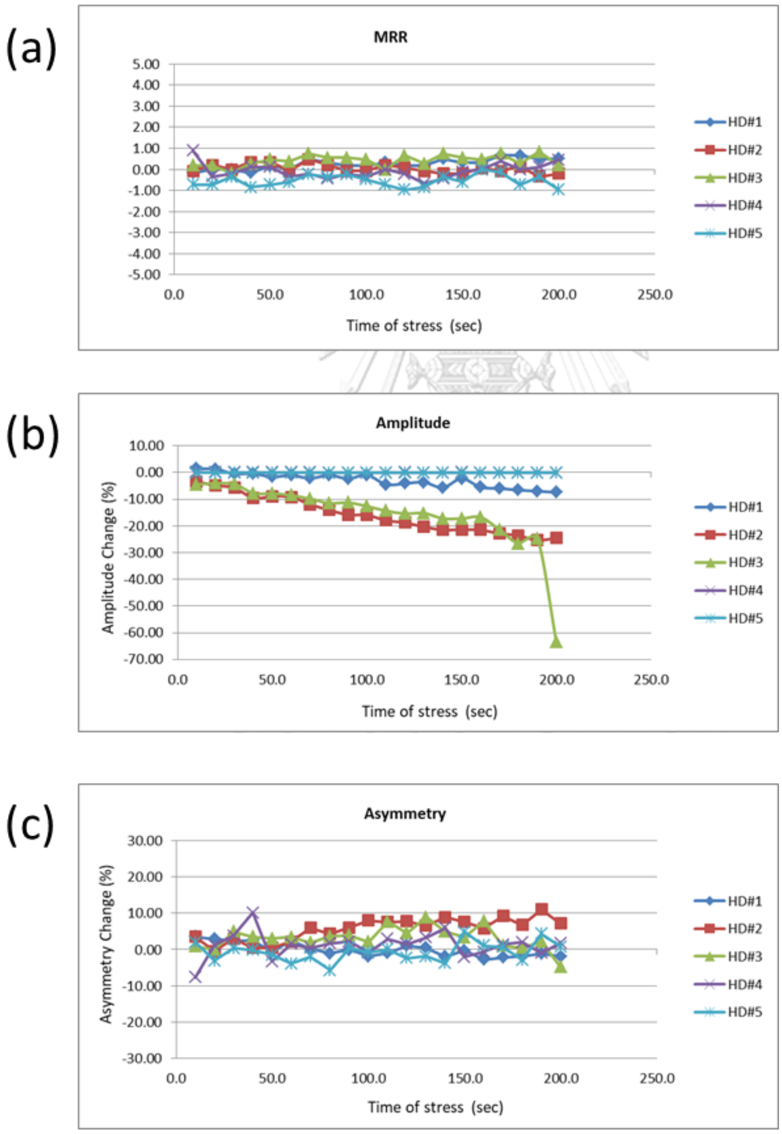

Fig. 5.8 QST percentage change parameter after laser stress; (a) MRR parameter, (b) amplitude parameter and (c) asymmetry parameter.

The QST amplitude decreasing is possibly due to heat generated of laser beam onto TMR area which high enough to make change in magnetic property of the TMR that could be observed the lower TMR response, or amplitude degradation. The temperature of stress on TMR device was calculated by using COMSOL MUTIPHYSIC software. It was found that the stress temperature on the TMR structure was about 427 ^{o}C. as shows in Fig. 5.9.

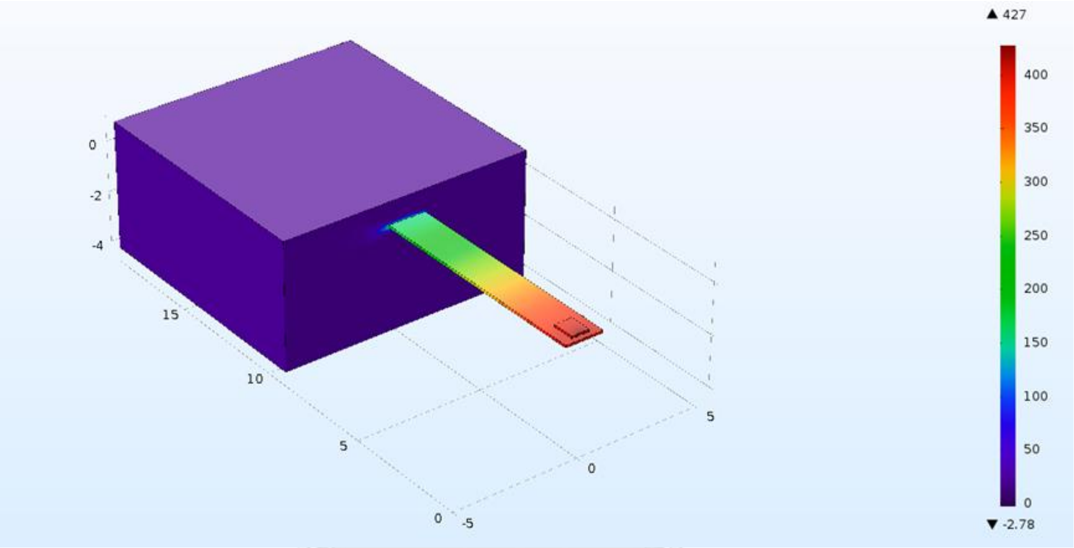

Fig. 5.9 Temperature calculation of laser beam stress on magnetic head by COMSOL MULTIPHYSIC, T ~ 427 ^{o}C on TMR area.

There has been reported that at the annealing temperature at of about 300 – 400 ^{o}C, boron (B) from CoFeB could diffuse into MgO layer, depending on the imperfect crystallite condition or pinhole on MgO layer [15, 16]. The MgO layer (barrier layer) is very critical layer to create electron tunneling effect of the TMR device, so if it has contamination such as B, the magnetic response could be reduced [13]. The amplitude degradation at about 427 ^{o}C by the laser stress was possibly cause B diffusion into MgO layer as one of the suspected potential root cause.

STEM images analysis results of the degradation TMR devices shows in Fig 5.10., all specimens of HD#1, HD#2 and HD#3 were hardly observed abnormality. The XEDS analysis results in Fig 5.11. shows Mn depletion on AFM layer, and very obvious *at air baring surface* (ABS), on the right hand side of the image. The function of AFM layer is to pin the pinned layer by magnetically exchange coupling. The pinned layer is required strongly fixed magnetization for reference angle to achieve the effective TMR effect. The depletion of Mn area could reduce effectiveness of the TMR because the magnetization of the pinned layer at that area could be moved freely, and cause none-active TMR zone as a result of amplitude degradation.

The stripe height (SH) and Mn depth were measured for calculation the AFM loss ratio as shows in Table 15.1., and do scatter plot graph with percentage of amplitude degradation as shows in Fig. 5.12. We found that degree of degradation depends on ratio of active and non-active zone for individual TMR element.

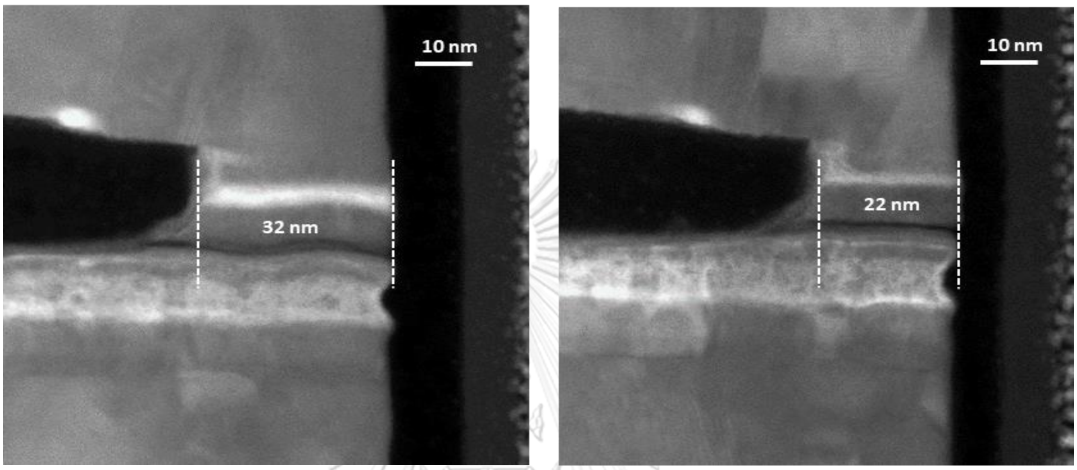

(a) STEM image of HD#1

(b) STEM image of HD#2

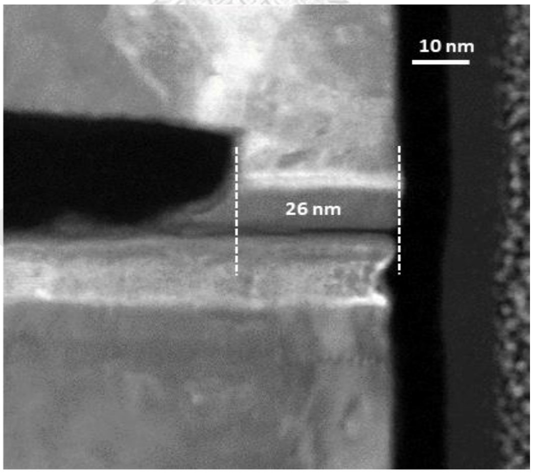

(c) STEM image of HD#3

Fig. 5.10 STEM images of (a) HD#1, (b) HD#2 and (c) HD#3.

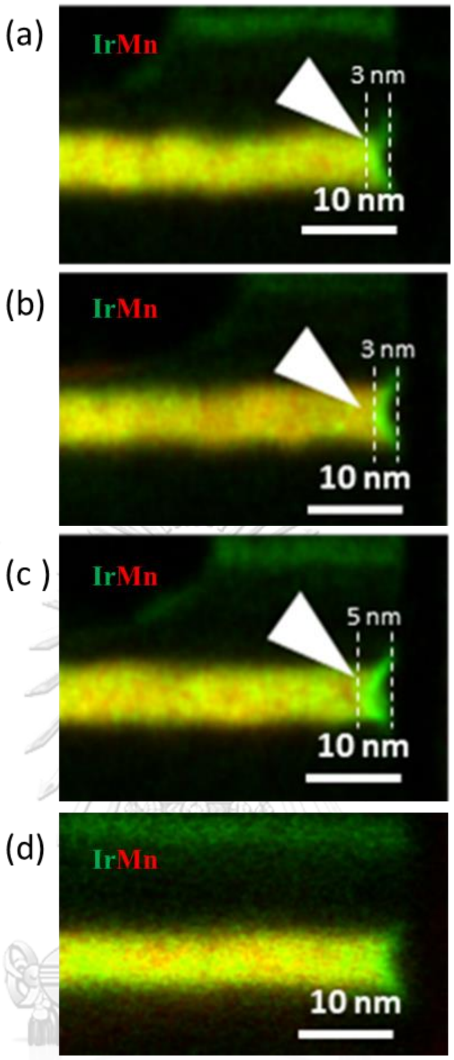

Fig. 5.11 XEDS analysis of (a) HD#1, (b) HD#2, (c) HD#3 and (d) Control head, observe Mn depletion on AFM layer.

Table 5.2 Stripe height, Mn depletion depth, AFM loss ratio and Amplitude degradation.

HD#	SH* (nm)	Mn_Deplition_Depth (nm)	AFM_Loss_Ratio	Amp_Degradation (%)
HD#1	32	3	0.09	-7.45
HD#2	22	3	0.14	-24.56
HD#3	26	5	0.19	-63.43

Note:
****SH : Stripe height***

AFM Loss Ratio = [Mn_Deplition_Depth] / [SH]

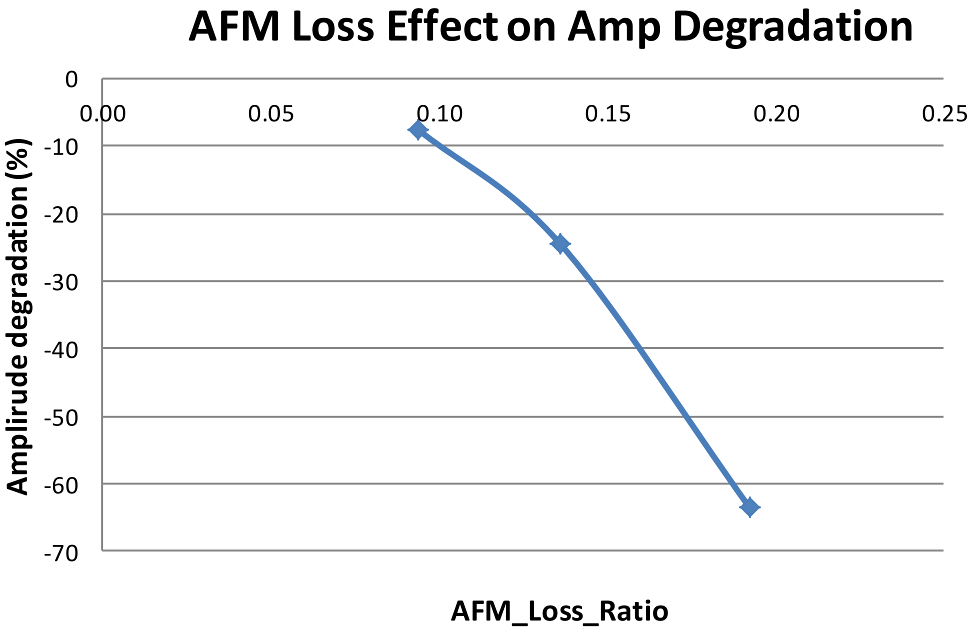

Fig. 5.12 Graph of amplitude degradation with AFM loss effect.

CHAPTER VI

CONCLUSIONS

The investigation of thermal stress influence on actual TMR stack structure in HDD recording head has been carried out by using QST measurement on the electromagnetism of the TMR reader structure. It was found that as the temperature increases, the percentage of change in resistance tends to increase. The percentage of change in asymmetry decreases while the percentage of change in amplitude exhibits both increasing and decreasing. We found that the degradation of MgO barrier layer and the Mn depletion in IrMn antiferromagnetic layer are the major reasons that cause the high percentage change in TMR resistance and some cases on the appearance of Barkhausen jump after the structure has been thermal stressed. This seems individual devices have individual characteristic, especially the defected devices. They would have obviously deviated from normal population after been thermally stressed.

On a unique characterization, the *in-situ* annealing STEM results showed the change in microstructure of the TMR stack after annealing above the temperature at about 250 ^{o}C. At 350 ^{o}C, the STEM micrograph showed some part of the interfaces of an ultra-thin Ru layer could not maintain an abrupt as the original structure (at 25 ^{o}C). This is a sign indicated a diffusion of top and bottom materials along the interfaces. The observation of changing at the ultra-thin Ru layer interface could also imply that other materials contained in TMR structure which have atomic weight lower than Ru (101.07) such as B (10.81), Fe (55.85), Ni (58.70), Co (58.93), Mg (24.31), O (15.99) and Mn (54.94), can diffuse to adjacent layers and causing the instability on TMR structure. We also found the structural deformation in the AFM layer at this stress temperature.

Considering the future technology on HAMR, the laser stress experiment on the TMR structure using 1,000 mW of 650 nm laser for 10 seconds, 20 cycle showed only the QST amplitude degradation when other QST parameters were not obviously changed. The temperature on TMR structure was about 427 ^{o}C, as calculated by using COMSOL MUTIPHYSIC. STEM and XEDS analysis results indicated Mn depletion in IrMn antiferromagnetic (AFM) layer, especially at ABS area, where the laser spot was radiated on the surface. The loss of Mn atoms in IrMn material could reduce effectiveness of TMR behavior. It can cause magnetization of the pinned layer at this area to be moved freely, that cause non-active TMR zone. The main root cause in QST amplitude degradation from the laser induced stress can be due to this Mn depletion of AFM layer. Degree of degradation depends on ratio of active and non-active zone for individual TMR element.

REFERENCES

1. Surawanitkun C, Kaewrawang A, Siritaratiwat A, Kruesubthaworn A, Sivaratana R, Jutong N, et al. Magnetic instability in tunneling magnetoresistive heads due to temperature increase during electrostatic discharge. 2012;12(3):570-5.
2. Marongmued K, Sa-ngiamsak CJA-PJoS, Technology. Shrinking size effects of CPP-TMR and CPP-GMR heads: failure phenomena caused by electrostatic discharge. 2012;17(3):348-57.
3. Han G, Qiu J, Wang L, Yeo W, Wang CJIToM. Perspectives of read head technology for 10 Tb/in $^{2} $ recording. 2010;46(3):709-14.
4. Wang W, Liu E, Kodzuka M, Sukegawa H, Wojcik M, Jedryka E, et al. Coherent tunneling and giant tunneling magnetoresistance in Co 2 FeAl/MgO/CoFe magnetic tunneling junctions. 2010;81(14):140402.
5. Zhu J-GJ, Park CJMt. Magnetic tunnel junctions. 2006;9(11):36-45.
6. Fernandez-Outon LE, O'Grady K, Oh S, Zhou M, Pakala MJIToM. Large exchange bias IrMn/CoFe for magnetic tunnel junctions. 2008;44(11):2824-7.
7. Int'l. IS. QST-2002 User's Manual2012. 175 p.
8. Mao S, Chen Y, Liu F, Chen X, Xu B, Lu P, et al. Commercial TMR heads for hard disk drives: characterization and extendibility at 300 gbit/in/sup 2. 2006;42(2):97-102.
9. Lee J, Jeong H, Kyung H, Yoon C, Kim C, Park BG, et al. Failure of exchange-biased low resistance magnetic tunneling junctions upon thermal treatment. 2002;91(1):217-20.
10. Miyajima T, Ito R, Honda K, Tsukada MJFS, Journal T. Evaluation of Devices and Materials by Transmission Electron Microscopy. 2010;46(3):273-9.
11. Baril L, Nichols M, Wallash AJItom. Degradation of GMR and TMR recording heads using very-short-duration ESD transients. 2002;38(5):2283-5.
12. Baril L, Higgins B, Wallash AJJoe. Effects of ESD transients on noise in tunneling recording heads. 2006;64(2):147-50.
13. Miyatake M, Kugiya F, Kodama NJIToD, Reliability M. ESD tolerance of GMR and TMR heads within Hard Disk Drives. 2010;10(4):476-81.
14. Matsugi J, Mizoh Y, Nakano T, Nakamura K, Sakakima HJItoepm. ESD phenomena in GMR heads in the manufacturing process of HDD and GMR heads. 2005;28(3):206-12.
15. Moodera JS, Santos TS, Nagahama TJJoPCM. The phenomena of spin-filter tunnelling. 2007;19(16):165202.
16. Schmidt GJJoPDAP. Concepts for spin injection into semiconductors—a review. 2005;38(7):R107.
17. Pertsev N, Kohlstedt HJAPL. Magnetic tunnel junction on a ferroelectric substrate. 2009;95(16):163503.
18. Tsymbal EY, Mryasov ON, LeClair PRJJoPCM. Spin-dependent tunnelling in magnetic tunnel junctions. 2003;15(4):R109.
19. Miyazaki T, Tezuka NJJom, materials m. Giant magnetic tunneling effect in Fe/Al2O3/Fe junction. 1995;139(3):L231-L4.
20. Moodera JS, Kinder LR, Wong TM, Meservey RJPrl. Large magnetoresistance at room temperature in ferromagnetic thin film tunnel junctions. 1995;74(16):3273.
21. Mao S, Nowak J, Song D, Kolbo P, Wang L, Linville E, et al. Spin tunneling

heads above 20 Gb/in/sup 2. 2002;38(1):78-83.
22. Mao S, Linville E, Nowak J, Zhang Z, Chen S, Karr B, et al. Tunneling magnetoresistive heads beyond 150 Gb/in/sup 2. 2004;40(1):307-12.
23. Butler W, Zhang X-G, Schulthess T, MacLaren JJPRB. Spin-dependent tunneling conductance of Fe| MgO| Fe sandwiches. 2001;63(5):054416.
24. Parkin SS, Kaiser C, Panchula A, Rice PM, Hughes B, Samant M, et al. Giant tunnelling magnetoresistance at room temperature with MgO (100) tunnel barriers. 2004;3(12):862.
25. Yuasa S, Nagahama T, Fukushima A, Suzuki Y, Ando KJNm. Giant room-temperature magnetoresistance in single-crystal Fe/MgO/Fe magnetic tunnel junctions. 2004;3(12):868.
26. Djayaprawira DD, Tsunekawa K, Nagai M, Maehara H, Yamagata S, Watanabe N, et al. 230% room-temperature magnetoresistance in CoFeB⁄MgO⁄CoFeB magnetic tunnel junctions. 2005;86(9):092502.
27. Wikipedia. Tunnel magnetoresistance [Online]. 2018 [cited 2018. Tunnel magnetoresistance]. Available from: https://en.wikipedia.org/wiki/Tunnel_magnetoresistance.
28. Julliere MJPlA. Tunneling between ferromagnetic films. 1975;54(3):225-6.
29. Naber WJM. Electron transport and spin phenomena in hybrid organic/inorganic systems: University of Twente [Host]; 2010.
30. Liu Y, Sellmyer DJ, Shindo D. Handbook of Advanced Magnetic Materials: Vol 1. Nanostructural Effects. Vol 2. Characterization and Simulation. Vol 3. Fabrication and Processing. Vol 4. Properties and Applications: Springer Science & Business Media; 2008.
31. Huang S, Chen T, Chien CJAPL. Spin polarization of amorphous CoFeB determined by point-contact Andreev reflection. 2008;92(24):242509.
32. Butler WHJS, Materials ToA. Tunneling magnetoresistance from a symmetry filtering effect. 2008;9(1):014106.
33. Tiusan C, Greullet F, Hehn M, Montaigne F, Andrieu S, Schuhl AJJoPCM. Spin tunnelling phenomena in single-crystal magnetic tunnel junction systems. 2007;19(16):165201.
34. Reiss G, Schmalhorst J, Thomas A, Hütten A, Yuasa S. Magnetic tunnel junctions. Magnetic Heterostructures: Springer; 2008. p. 291-333.
35. Kanak J, Stobiecki T, Thomas A, Schmalhorst J, Reiss GJV. Structural and tunneling properties of magnetic tunnel junctions with Al–O and MgO barrier. 2008;82(10):1057-61.
36. Yuasa S, Fukushima A, Kubota H, Suzuki Y, Ando KJAPL. Giant tunneling magnetoresistance up to 410% at room temperature in fully epitaxial Co⁄Mg O⁄Co magnetic tunnel junctions with bcc Co (001) electrodes. 2006;89(4):042505.
37. Yuasa S, Djayaprawira DJJoPDAP. Giant tunnel magnetoresistance in magnetic tunnel junctions with a crystalline MgO (0 0 1) barrier. 2007;40(21):R337.
38. Ando Y, Miyakoshi T, Oogane M, Miyazaki T, Kubota H, Ando K, et al. Spin-dependent tunneling spectroscopy in single-crystal Fe⁄Mg O⁄Fe tunnel junctions. 2005;87(14):142502.
39. Choi Y, Tsunekawa K, Nagamine Y, Djayaprawira DJJoap. Transmission electron microscopy study on the polycrystalline Co Fe B⁄Mg O⁄Co Fe B based magnetic tunnel junction showing a high tunneling magnetoresistance, predicted in

single crystal magnetic tunnel junction. 2007;101(1):013907.

40. Tsumekawa K, Djayaprawira D, Nagai M, Maehara H, Yamagata S, Watanabe N, editors. Effect of capping layer material on tunnel magnetoresistance in CoFeB-MgO-CoFeB magnetic tunnel junctions. Magnetics Conference, 2005 INTERMAG Asia 2005 Digests of the IEEE International; 2005: IEEE.

41. Lee Y, Hayakawa J, Ikeda S, Matsukura F, Ohno HJApl. Effect of electrode composition on the tunnel magnetoresistance of pseudo-spin-valve magnetic tunnel junction with a MgO tunnel barrier. 2007;90(21):212507.

42. Devasahayam A, Kryder MJJoap. The dependence of the antiferromagnet/ferromagnet blocking temperature on antiferromagnet thickness and deposition conditions. 1999;85(8):5519-21.

43. Nozieres J, Jaren S, Zhang Y, Zeltser A, Pentek K, Speriosu VJJoAP. Blocking temperature distribution and long-term stability of spin-valve structures with Mn-based antiferromagnets. 2000;87(8):3920-5.

44. Aley N, O'Grady KJJoAP. Compositional dependence of antiferromagnetic anisotropy in IrMn/CoFe exchange bias systems. 2011;109(7):07D719.

45. Rodríguez-Suárez R, Vilela-Leão L, Bueno T, Oliveira A, de Almeida J, Landeros P, et al. Critical thickness investigation of magnetic properties in exchange-coupled bilayers. 2011;83(22):224418.

46. Kerr E, van Dijken S, Coey JJJoap. Influence of the annealing field strength on exchange bias and magnetoresistance of spin valves with IrMn. 2005;97(9):093910.

47. Wikipedia. Barkhausen effect 2018 [cited 2018. Barkhausen effect]. Available from: https://en.wikipedia.org/wiki/Barkhausen_effect.

48. Oliver B, Tuttle G, He Q, Tang X, Nowak JJJoap. Two breakdown mechanisms in ultrathin alumina barrier magnetic tunnel junctions. 2004;95(3):1315-22.

49. Khan AA, Schmalhorst J, Thomas A, Schebaum O, Reiss GJJoAP. Dielectric breakdown in Co–Fe–B/MgO/Co–Fe–B magnetic tunnel junction. 2008;103(12):123705.

50. Velev JP, Belashchenko KD, Jaswal SS, Tsymbal EYJAPL. Effect of oxygen vacancies on spin-dependent tunneling in Fe∕Mg O∕Fe magnetic tunnel junctions. 2007;90(7):072502.

51. Xi H, Franzen S, Guzman JI, Mao SJJoM, Materials M. Degradation of magnetic tunneling junctions caused by pinhole formation and growth. 2007;319(1-2):60-3.

52. Thomas A, Drewello V, Schäfers M, Weddemann A, Reiss G, Eilers G, et al. Direct imaging of the structural change generated by dielectric breakdown in MgO based magnetic tunnel junctions. 2008;93(15):152508.

53. Dimitrov D, Gao Z, Wang X, Jung W, Lou X, Heinonen OGJAPL. Dielectric breakdown of MgO magnetic tunnel junctions. 2009;94(12):123110.

54. Victora R, Chen XJIToM. Predicted effects of pinhole and surface roughness in magnetoresistive read head. 2010;46(3):702-8.

55. Wikipedia. Transmission electron microscopy [Online]. 2018 [cited 2018. Transmission electron microscopy]. Available from: https://en.wikipedia.org/wiki/Transmission_electron_microscopy.

56. Wikipedia. Focused ion beam [Online]. 2018; 2018 [Focused ion beam]. Available from: https://en.wikipedia.org/wiki/Focused_ion_beam.

57. Wikipedia. Energy-dispersive X-ray spectroscopy [Online]. 2018 [cited 2018.

Energy-dispersive X-ray spectroscopy]. Available from: https://en.wikipedia.org/wiki/Energy-dispersive_X-ray_spectroscopy.

VITA

NAME	Pornchai Rakpongsiri
DATE OF BIRTH	22 Nov 1967
PLACE OF BIRTH	Hhon_Kaen
INSTITUTIONS ATTENDED	Chiang Mai University
HOME ADDRESS	59/92 Than-Man-Kong Khlong Song Khlong Luang Pathumthani Postcode 12120
PUBLICATION	[1] Rakpongsiri, P., Pintasiri, S., Ruthe, K., Persson, P.O.A, and Tungasmita S., Thermal Stress Evaluation of Tunneling Magnetoresistive Structures in Data Storage Devices, IEEE MAGNETICS LETTERS, Magneto-Electronics, 2018. 9: p. 1-4. [2] Rakpongsiri, P., Tungasmita, S., Effect of Laser Stress on Tunneling Magnetoresistive Structure, (manuscript, plan to publish in Journal of Applied Physics).